EurJIC
European Journal of Inorganic Chemistry

Full Paper
doi.org/10.1002/ejic.202000435

Cobalt Clusters

Temperature-Sensitive Structural Speciation of Cobalt-Iminodialcohol-(N,N′-Aromatic Chelator) Systems: Lattice Architecture and Spectrochemical Properties

Sevasti Matsia,[a] Melita Menelaou,[a] Antonios Hatzidimitriou,[b] Vassilis Tangoulis,[c] Nikolia Lalioti,[c] Nikolaos Ioannidis,[d] Laura Blömer,[e] Berthold Kersting,[e] and Athanasios Salifoglou*[a]

Abstract: Temperature-sensitive crystalline phases, pertaining to discrete clusters of binary and ternary Co(II,III):iminodipropanol:(N,N′-aromatic binder) systems, were prepared. The rich structural speciation of such systems in alcoholic media and their unique structural, magnetic, and spectroscopic profiles have been demonstrated. The need to understand the chemical reactivity of such complex ternary Co(II)-(1,1′-iminodi-2-propanol) systems, in the presence of N,N′-aromatic chelators 2,2′-bipyridine and 1,10-phenanthroline and aromatic binder 4,4′-bipyridine in methanol, led to the synthetic development of well-defined hybrid metal-organic materials with discrete spectroscopic, structural, electrochemical, and magnetic properties. The surprisingly plethoric family of the prepared mononuclear-trinuclear-tetranuclear Co(II,III) clusters was characterized through elemental analysis, FT-IR, and X-ray crystallography. Enrichment of their physicochemical profile originated from electrochemical, optical (UV/Vis, luminescence), magnetic, and EPR studies, unequivocally supporting their structural formulation. Collectively, the experimentally and theoretically (Bond-Valence-Sum, Hirshfeld) perused structures project the influence of molecular stoichiometry and temperature on targeted synthetic efforts toward crystal engineering of discrete Co(II,III)-center assemblies, exemplifying structure-reactivity correlations and magneto-optical-structural attributes.

Introduction

Variable nuclearity clusters have been at the forefront of coordination chemistry due to their broad spectrum of applications in catalysis,[1,2] nanoscience,[3–5] optoelectronics,[6,7] magneto-optics[8–13] and the biological-environmental field.[14–17] Coordination compounds arising from the design and synthetic routes between transition metal ions and appropriately-configured organic ligands are of great interest[18–20] in all of the above fields. Advancements, in that respect, rely heavily on the nature of organic ligands seeking interaction(s) with appropriately chosen metal ions at the binary and/or ternary level. Among those metal ions, cobalt attracts considerable attention, because of the a) wide range of stable geometries it can assume in the emerging clusters, b) high magneto-crystalline anisotropy characterizing the generated assemblies, and c) diverse chemical reactivity it can accommodate with a large pool of variable structure and molecular mass ligands.[8,21] Complex assemblies of different nuclearity, involving both cobalt oxidation states (Co(II) and Co(III)) and multidentate ligands, have thus been achieved and a wealth of magnetic properties have been unraveled to project potential applications in fields such as Single-Molecule Magnets (SMMs).[12,22–29]

Given the importance of ligand structure in the design of such materials, amino alcohols possess key such reactivity groups poised to seek metal ion complexation, thus promoting assembly of oligonuclear clusters. Consequently, the chemical reactivity of Co(II,III) ion toward neutral (O,N,O)-terminal containing (amino)alcohol and carboxylic acid ligands stands as the basis for the development of materials exemplifying the diversity of structural motifs possessing specified physicochemical attributes.[30–36] Among such attributes included are the a) nuclearity of the cluster assembly at the binary-ternary metal-organic level, b) structural composition of the arising metal ionic assembly, c) molecular stoichiometry among the partners in the investigated systems, and d) the defined solvent system (e.g. alcohol) in which the chemical reactivity is probed into, with

[a] S. Matsia, Dr. M. Menelaou, Prof. A. Salifoglou
School of Chemical Engineering, Aristotle University of Thessaloniki, Thessaloniki 54124, Greece
E-mail: salif@auth.gr
http://bioinorglab.web.auth.gr/en_site/page1en.htm
[b] Prof. A. Hatzidimitriou
Department of Chemistry, Aristotle University of Thessaloniki, Thessaloniki 54124, Greece
[c] Prof. V. Tangoulis, Dr. N. Lalioti
Department of Chemistry, Laboratory of Inorganic Chemistry, University of Patras,
Patras 26504, Greece
[d] Dr. N. Ioannidis
Institute of Nanoscience and Nanotechnology, NCSR "Demokritos", Aghia Paraskevi 15310, Attiki, Greece
[e] Dr. L. Blömer, Prof. B. Kersting
Institut für Anorganische Chemie, Universität Leipzig, Johannisallee 29, Leipzig, 04103, Germany
Supporting information and ORCID(s) from the author(s) for this article are available on the WWW under https://doi.org/10.1002/ejic.202000435.

Full Paper
doi.org/10.1002/ejic.202000435

the oxidation state of the various metal centers playing a key role in the formulation of optical and magnetic properties in the emerging (oligo, multi)nuclear assemblies.

Often, serendipity or other ill-understood or defined factors (such as thermodynamics) lead to the synthesis and isolation of such clusters. To that end, the rational design of such assemblies and their associated lattice architectures remain a challenge, providing a well-defined impetus to synthesizing new binary-ternary materials bearing distinctly differentiated electronic-magnetic properties.

Driven by the scarcely encountered rationale entering the design and synthesis of such well-defined materials, research was launched in our labs to pursue hybrid metal-organic materials bearing distinct structural and magneto-optical correlations in the first transition metal ion series. The investigation relied on the a) general ternary Co(II):(1,1′-iminodi-2-propanol):(N,N′-aromatic chelator) system, and b) introduction of parameters-factors that could influence the chemical reactivity of Co(II) toward select iminodialcohol ligands (Scheme 1) under defined molecular stoichiometry and temperature-specific conditions.

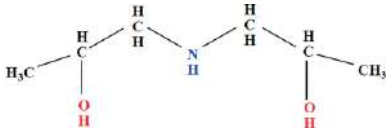

Scheme 1. Di-alcoholic 1,1′-iminodi-2-propanol ligand employed in the study.

The experimental and theoretical results exemplify the diversity of the chemical reactivity studied and project distinct correlations involving the aforementioned factors, all useful in a) rationalizing the importance of structural speciation in a ternary metal-organic system linked to crystalline cluster synthesis and isolation, and b) identifying the salient features entering the design of new metal-organic hybrid materials with specific electronic and magnetic properties.

Results

Syntheses

All compounds **1**–**6** were synthesized through simple reactions between a divalent metal ion (M(II) = Co) and a representative (imino)alcohol 1,1′-iminodi-2-propanol (H_3L), employing variable molar ratios. The diversity of Co(II,III) assemblies in the emerging different compounds was investigated through the properties of the different aromatic chelators. Specifically:

Dark red crystalline compound $[Co^{II}_2Co^{III}_2(OH)(CH_3O)(C_6H_{12.5}NO_2)_2(C_{10}H_8N_2)_2(NO_3)_2](NO_3)\cdot 3CH_3OH\cdot H_2O$ (**1**) was synthesized through a simple reaction between $Co(NO_3)_2\cdot 6H_2O$, 1,1′-iminodi-2-propanol (H_3L) and 2,2′-bipy in methanol with a molar ratio of 1:1:1 or 2:1:1 at 25°C. The overall stoichiometric reaction leading to **1** is shown below.

A dark red mixture of crystalline compounds $[Co^{II}Co^{III}_2(H_2O)(OH)(C_6H_{13}NO_2)_2(C_{10}H_8N_2)_3](NO_3)_3\cdot 2CH_3OH$ (**2**) and $[Co^{II}Co^{III}_2(OH)_2(C_6H_{14}NO_2)_2(C_{10}H_8N_2)_3](NO_3)_4\cdot CH_3OH$ (**3**) was obtained through an analogous reaction between $Co(NO_3)_2\cdot 6H_2O$,

1,1′-iminodi-2-propanol (H_3L) and 2,2′-bipy in methanol with a molar ratio of 1:1:1 at 4°C. The overall stoichiometric reaction leading to **2** and **3** is shown below.

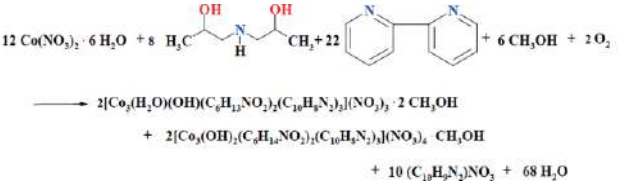

In an analogous reactivity pattern, dark brown crystalline compound $[Co^{II}_2Co^{III}_2(OH)_2(C_6H_{12.5}NO_2)_2(C_{12}H_8N_2)_3(NO_3)](NO_3)_2\cdot 3CH_3OH$ (**4**) was synthesized through a reaction of $Co(NO_3)_2\cdot 6H_2O$ with 1,1′-iminodi-2-propanol (H_3L) and 1,10-phen, in a molar ratio 1:1:1, in methanol solution at 25°C and 4°C. The overall stoichiometric reaction leading to **4** is shown below.

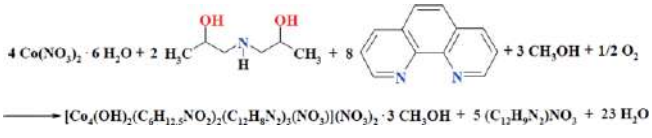

Through the same line of thinking, the reaction between $Co(NO_3)_2\cdot 6H_2O$ with 1,1′-iminodi-2-propanol (H_3L) and 1,10-phen in a molar ration 2:1:1 led to the isolation of a different material compared to **4**. The reaction below indicates the stoichiometry leading to $[Co^{II}_2Co^{III}_2(OH)_2(C_6H_{13}NO_2)_2(C_{12}H_8N_2)_2(NO_3)_2](NO_3)_2\cdot 2.5H_2O$ (**5**).

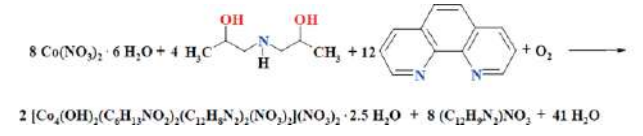

In all cases, the aromatic chelator binders 2,2′-bipy (**1, 2, and 3**) and 1,10-phen (**4, 5**) were employed, with both ligands proven crucial for the isolation of crystalline material(s) and further characterization. Methanol was also a crucial point for achieving a stable lattice. The arising mixed Co(II,III)-(1,1′-iminodi-2-propanol) species were retrieved in pure crystalline form upon slow evaporation.

In contrast to what had thus far been observed, the reactivity between $Co(NO_3)_2\cdot 6H_2O$ with 1,1′-iminodi-2-propanol (H_3L) and 4,4′-bipy shows a different coordination composition around the metal ion, including the aromatic binder and nitrate ions. The 1,1′-iminodi-2-propanol ligand, is not coordinated to Co(II). The stoichiometric reaction leading to $[Co^{II}(C_{10}H_8N_2)(NO_3)_2(H_2O)_2]_n\cdot nH_2O$ (**6**) is shown below.

Full Paper
doi.org/10.1002/ejic.202000435

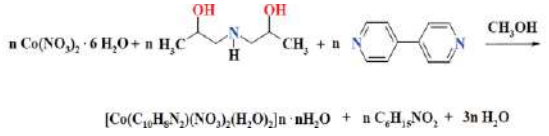

$$n\,Co(NO_3)_2\cdot 6H_2O + n\,H_3C(OH)CH(NH)CH(OH)CH_3 + n\,C_{10}H_8N_2 \xrightarrow{CH_3OH} [Co(C_{10}H_8N_2)(NO_3)_2(H_2O)_2]_n\cdot nH_2O + n\,C_6H_{15}NO_2 + 3n\,H_2O$$

It appears that the chemical reactivity of the different aromatic binders with the ligand (H_3L) and cobalt ion is crucial for the isolation of crystalline materials **1–6**.

Elemental analysis on all reproducibly isolated crystalline products suggested the molecular formulation **1, 4–6**. In the case of compounds **2** and **3**, discrete phases were reproducibly obtained and accounted for through FT-IR and X-ray crystallography. Further spectroscopic evaluation of the crystalline products by FT-IR confirmed the presence of 1,1′-iminodi-2-propanol ligand and the aromatic chelator bound to the metal ion(s) in all materials except **6**. Finally, X-ray crystallography confirmed the analytical and spectroscopic results by providing the molecular formulation of the crystalline materials **1–6**.

Description of X-ray Crystallographic Structures

Crystallographic data for all compounds **1–6** are presented in Table 1.

Compound **1** crystallizes in the orthorhombic Pccn crystallographic space system. Crystallographic bond lengths and angles are shown in Table 2 and Table S1. It is a mixed valence-mixed ligand tetranuclear cluster. The moiety formula $C_{33}H_{45}Co_4N_8O_{12}$, $3(CH_4O)$, NO_3, H_2O comprises a main singly cationic tetranuclear core $[Co_4(OH)(CH_3O)(C_6H_{12.5}NO_2)_2(C_{10}H_8N_2)_2(NO_3)_2]^+$ assembly (Figure 1**A**), one nitrate counter anion, three solvate methanol molecules and one lattice water molecule. The tetranuclear assembly consists of four cobalt ions symmetrically generated with respect to the center of symmetry in the mid distance Co(2)–Co(2)′, both sitting on special positions. These two cobalt ions are Co(II) centers, with the pair of the remaining cobalt centers being Co(III). The oxidation state assignments for the cobalt centers were made using charge considerations, Bond Valence Sum (BVS) calculations, and inter-

Table 1. Summary of crystallographic data on compounds $[Co^{II}_2Co^{III}_2(OH)(CH_3O)(C_6H_{12.5}NO_2)_2(C_{10}H_8N_2)_2(NO_3)_2](NO_3)\cdot 3CH_3OH\cdot H_2O$ **(1)**, $[Co^{II}Co^{III}_2(H_2O)(OH)(C_6H_{13}NO_2)_2(C_{10}H_8N_2)_3](NO_3)_3\cdot 2CH_3OH$ **(2)**, $[Co^{II}Co^{III}_2(OH)_2(C_6H_{14}NO_2)_2(C_{10}H_8N_2)_3](NO_3)_4\cdot CH_3OH$ **(3)**, $[Co^{II}_2Co^{III}_2(OH)_2(C_6H_{12.5}NO_2)_2(C_{12}H_8N_2)_3(NO_3)](NO_3)_2\cdot 3CH_3OH$ **(4)**, $[Co^{II}_2Co^{III}_2(OH)_2(C_6H_{13}NO_2)_2(C_{12}H_8N_2)_2(NO_3)_2](NO_3)_2\cdot 2.5H_2O$ **(5)**, $[Co^{II}(C_{10}H_8N_2)(NO_3)_2(H_2O)_2]_n\cdot nH_2O$ **(6)**.

Compound	1	2	3	4	5	6
Chemical formula	$C_{36}H_{59}Co_4N_9O_{19}$	$C_{44}H_{53}Co_3N_{11}O_{17}$	$C_{43}H_{58}Co_3N_{12}O_{19}$	$C_{51}H_{56}Co_4N_{11}O_{18}$	$2[C_{36}H_{49}Co_4N_{10}O_{20.50}]$	$C_{10}H_{14}CoN_4O_9$
M_r	1157.65	1184.77	1223.80	1346.80	2 × 1185.57	393.18
Crystal system	Orthorhombic	Monoclinic	Monoclinic	Monoclinic	Triclinic	Orthorhombic
Space group	*Pccn*	*C*2/*c*	$P2_1$	*C*2/*c*	$P\bar{1}$	*Cccm*
Temperature (K)	295	295	295	295	295	295
a (Å)	17.1261(6)	13.4628(5)	9.5944(12)	14.1241(6)	11.8990(10)	11.7615(9)
b (Å)	19.2572(7)	21.7564(8)	22.060(3)	19.3903(8)	12.3082(13)	19.4549(11)
c (Å)	16.2533(5)	18.8778(9)	13.1225(17)	23.3541(13)	19.890(2)	7.3905(5)
α (°)	90	90	90	90	103.127(3)	90
β (°)	90	100.695(2)	102.329(4)	106.306(2)	102.227(3)	90
γ (°)	90	90	90	90	104.604(3)	90
V (Å^3)	5360.4(3)	5433.3(4)	2713.4(6)	6138.7(5)	2631.0(5)	1691.1(2)
Z	4	4	2	4	2 × 1	4
Radiation type	Mo *K*α	Mo *K*α	Mo *K*α	Mo *K*α	Mo *K*α	Mo *K*α
μ (mm^{-1})	1.29	0.98	0.99	1.14	1.32	1.07
Crystal size (mm)	0.16 × 0.19 × 0.28	0.24 × 0.23 × 0.10	0.22 × 0.17 × 0.07	0.14 × 0.19 × 0.22	0.15 × 0.17 × 0.25	0.16 × 0.24 × 0.26
Data collection						
Diffractometer	Bruker Kappa APEX II	Bruker Kappa APEX II	Bruker Kappa APEX II	Bruker Kappa APEX II	Bruker Kappa APEX II	Bruker Kappa APEX II
Absorption correction	Numerical	Numerical	Numerical	Numerical	Numerical	Numerical
T_{min}, T_{max}	0.78, 0.81	0.72, 0.91	0.85, 0.93	0.81, 0.85	0.80, 0.82	0.77, 0.84
Reflections						
No. of measured	28718	21725	42178	24177	59286	3555
independent	5307	5565	11029	6077	11027	902
observed [$I > 2.0\sigma(I)$]	3478	3575	7492	4275	8320	744
R_{int}	0.027	0.022	0.036	0.026	0.016	0.028
$(\sin\theta/\lambda)_{max}$ (Å^{-1})	0.621	0.628	0.627	0.618	0.640	0.619
Refinement						
$R[F^2 > 2\sigma(F^2)]$	0.054	0.040	0.033	0.052	0.049	0.054
R_w (F^2)	0.099	0.084	0.070	0.107	0.074	0.118
S	1.000	1.000	1.000	1.000	1.000	1.000
No. of reflections	3478	3575	7492	4246	8320	744
No. of parameters	318	343	695	390	649	71
No. of restraints	5	3	1	4	0	12
$\Delta\rho_{max}$, $\Delta\rho_{min}$ (e Å^{-3})	0.56, −0.44	0.60, −0.37	0.60, −0.30	0.74, −1.01	0.77, −0.42	0.62, −1.03

Full Paper
doi.org/10.1002/ejic.202000435

Table 2. Selected crystallographic data on compounds **1–6**.

			Bond lengths (Å)		
1		**2**		**3**	
Co(1)–O(1)	1.887(3)	Co(1)–O(3)	2.151(2)	Co(1)–N(1)	1.919(4)
Co(1)–O(3)	1.949(3)	Co(1)–N(4)	2.126(3)	Co(1)–O(2)	1.897(3)
Co(1)–N(1)	1.923(4)	Co(1)–O(1)	2.086(2)	Co(2)–O(3)	1.880(3)
Co(2)–O(4)	2.147(4)	Co(3)–O(1)	1.878(2)	Co(2)–O(4)	1.927(3)
Co(2)–O(3)	2.099(3)	Co(3)–O(3)	1.911(2)	Co(3)–O(6)	2.143(3)
Co(2)–O(5)	2.197(4)	Co(3)–N(1)	1.931(3)	Co(3)–N(7)	2.093(4)
4		**5**		**6**	
Co(1)–O(3)	1.932(3)	Co(1)–O(1)	2.055(2)	Co(1)–O(2)	2.155(7)
Co(1)–O(1)	1.887(3)	Co(2)–O(1)	1.896(2)	Co(1)–N(1)	2.136(5)
Co(1)–N(2)	1.976(4)	Co(2)–N(2)	1.986(3)	O(2)–N(2)	1.262(8)
Co(2)–O(2)	2.071(3)	Co(3)–O(7)	2.032(2)	O(4)–N(2)	1.242(7)
Co(2)–N(4)	2.102(4)	Co(4)–O(8)	1.915(2)		
Co(3)–O(4)	2.150(3)	Co(4)–N(4)	1.942(3)		
			Angles (°)		
1		**2**		**3**	
O(1)–Co(1)–O(2)	94.03(14)	O(1)–Co(1)–O(3)	73.34(8)	N(1)–Co(1)–N(3)	95.48(17)
O(2)–Co(1)–N(1)	87.25(15)	O(1)–Co(1)–N(4)	95.33(11)	N(1)–Co(1)–O(1)	85.81(14)
N(1)–Co(1)–N(2)	93.99(17)	N(1)–Co(3)–N(2)	92.89(13)	O(1)–Co(1)–O(2)	93.86(13)
O(1)–Co(2)–O(3)	76.27(12)	O(3)–Co(3)–N(3)	93.20(11)	N(2)–Co(2)–O(3)	87.32(14)
O(4)–Co(2)–O(5)	59.70(16)			N(8)–Co(3)–O(3)	100.21(14)
				O(3)–Co(3)–O(6)	74.07(11)
4		**5**		**6**	
O(1)–Co(1)–O(2)	95.62(12)	O(1)–Co(1)–O(3)	76.92(9)	$O(2)^{i}$–Co(1)–$O(2)^{ii}$	95.3(4)
O(2)–Co(1)–N(1)	87.16(14)	O(1)–Co(2)–N(1)	87.65(13)		
N(1)–Co(1)–N(2)	92.85(16)	N(1)–Co(2)–N(2)	94.43(14)	$O(2)^{i}$–Co(1)–N(1)	94.5(2)
O(3)–Co(3)–O(4)	106.14(11)	O(1)–Co(2)–N(3)	174.55(11)	O(2)–Co(1)–N(1)	85.5(2)
		O(7)–Co(3)–O(10)	93.20(11)	Co(1)–O(2)–N(2)	128.8(5)
		O(7)–Co(4)–N(4)	86.86(15)	(i) –x + 1/2, –y + 3/2, –z + 1	
		N(5)–Co(4)–N(6)	84.22(14)	(ii) –x + 1/2, –y + 3/2, z	

atomic distances (Co(II,III)–N and Co(II,III)–O). To that end, calculations revealed BVS values of 1.947 for Co(II) (Co(2)) and 3.125 Co(III) (Co(1)) centers. Of the two iminodipropanol ligands, one is doubly deprotonated and the second one is triply deprotonated. Two 2,2′-bipyridine (2,2′-bipy) ligands are each coordinated to one Co(III) center in a bidentate chelating mode through both of their nitrogen atoms. The two nitrate anions are each coordinated to one Co(II) ion in a bidentate chelating fashion through both of their oxygen atoms. In the tetranuclear core, there are also two more anions, one hydroxido and one methoxido, both bridging two Co(II) and one Co(III) cations though their oxygen anchors. The hydroxido and methoxido bridges were found disordered with occupancy factors 0.5 over two equivalent positions. The oxygen atom in both anions was found being fully occupied with the hydrogen atom changing position with the methyl group. The iminodipropanol ligands were also found to be disordered. The imine hydrogen was found with an occupancy factor 0.5, consequently rendering the ligand doubly or triply deprotonated over two equivalent positions.

The geometry around each cobalt ion is distorted octahedral. Each Co(III) center (Co(1), Co(1′)) is coordinated to three nitrogen and three oxygen atoms. The nitrogen atoms originate in the 2,2′-bipy and iminodipropanol ligands. One of the oxygen atoms originates from a disordered hydroxido and/or a methoxido anion. The remaining two oxygens come from an iminodipropanol ligand. These oxygen atoms are bridging the Co(III) and Co(II) ions of the asymmetric unit. Each Co(II) (Co(2), Co(2′)) is connected to six oxygen atoms. Two of them come from one of the bridging deprotonated alcoholic oxygens of the iminodipropanol ligand and its symmetry generated counterpart. Two more come from the bidentate nitrato ligand. The remaining two oxygens originate from the triply bridging disordered hydroxido moiety and the symmetry generated methoxido anion.

Figure 1 **A** exhibits the tetranuclear singly cationic assembly with iminodipropanolato, hydroxido and methoxido ligands occupying one of their two equivalent positions. The Co(III)–O distances vary from 1.887(3) to 1.949(4) Å, with Co(III)–N distances varying from 1.923(4) to 1.957(4) Å as expected.[37] The Co(II)–O distances vary from 2.026(3) to 2.197(4) Å, typical values for Co(II)–O distances.[38,39]

Hydrogen-bonding interactions are either simply keeping the lattice solvent molecules (O(11) to O(12)) together or bridging other lattice solvent molecules and the hydroxido and/or methoxido anionic ligands of the core assembly (O(3), O(9), O(10)). They finally form zig-zag chains parallel to the diagonal of the a0b plane. The so formed lattice architecture (Figure 1**B**–**C**) can be described as one dimensional (1D)..

Full Paper
doi.org/10.1002/ejic.202000435

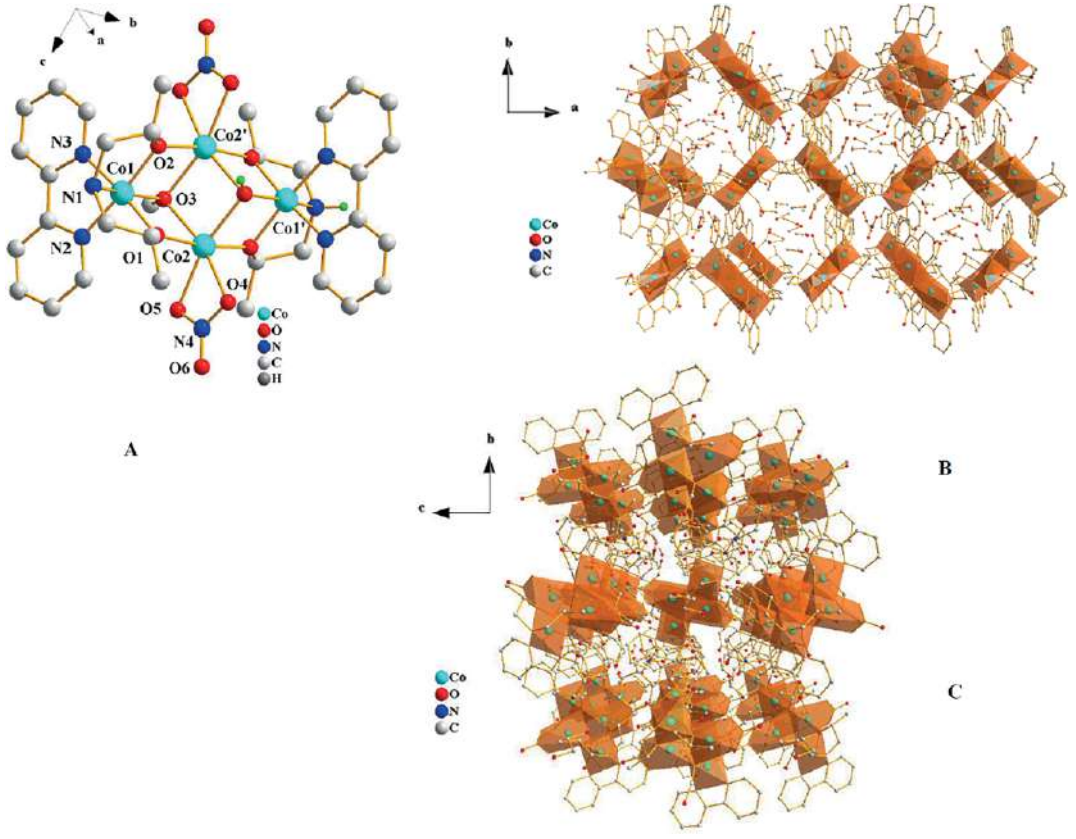

Figure 1. **A.** Diamond plot of cluster assembly $[Co_4(OH)(CH_3O)(C_6H_{12.5}NO_2)_2(C_{10}H_8N_2)_2(NO_3)_2]^+$ in **1**. **B**. Lattice of **1** in the *ab* plane. **C**. Lattice of **1** in the *bc* plane.

Compound **2** crystallizes in the monoclinic *C*2/*c* space group. Crystallographic bond lengths and angles are shown in Table 2 and Table S1. The moiety formula $[Co^{II}Co^{III}_2(H_2O)(OH)(C_6H_{13}NO_2)_2(C_{10}H_8N_2)_3](NO_3)_3{\cdot}2CH_3OH$ describes the existence of one triply cationic trinuclear cobalt assembly (Figure 2**A**), with three nitrates as counter anions and two severely disordered methanol solvate molecules (Figure 2**B–C**), with their oxygen atoms occupying one special and four general positions. The total multiplicity of the site is four.

The trinuclear mixed ligand-mixed valence complex assembly contains one Co(II) (Co(1)) sitting on a special position and two Co(III) (Co(3), Co(3)′) ions placed on general positions, one water ligand and one hydroxido ligand, two iminodipropanolato doubly deprotonated dianions and three 2,2′-bipy ligands, all symmetrically correlated with respect to the C_2 symmetry axis passing through Co(1) and the sigma bond mid-distance of the 2,2′-bipy coordinated to Co(1). The 2,2′-bipy ligands are coordinated in a typical bidentate chelate mode, one around each metal ion. Doubly deprotonated iminodipropanol ligand oxygen atoms are bound one to a Co(III) ion only, with the second one bridging one Co(III) and the Co(II) center. The ligand is also coordinated to Co(III) through the protonated nitrogen atom. The oxidation state assignments for the cobalt centers were supported through BVS calculations, revealing values of 1.853 for Co(II) (Co(1)) and 2.795 for Co(III) (Co(3)), respectively. Finally, two oxygen atoms, one from the ligated water molecule and one from the hydroxido anionic ligand were found disordered and alternating over the respective positions between them, while bridging each Co(III) to the central Co(II) ion. All metal ions have a distorted octahedral environment of coordinated atoms. Each Co(III) center is connected to three nitrogen and three oxygen atoms, with Co(II) being connected to two nitrogen and four oxygen atoms.

Figure 2 **A** displays the trinuclear tricationic complex assembly. The Co(II)–O distances vary from 2.086(2) to 2.151(2) Å, whereas Co(II)–N distances were both found to be 2.126(3) Å due to symmetry considerations. All distances have the expected values.[40] The Co(III)–O distances vary from 1.878(2) to 1.929(2) Å, with Co(III)–N distances varying from 1.931(3) to 1.938(3) Å, all typical values for Co(III)-(O,N) distances.[40]

Hydrogen-bonding interactions emerge between the bound water and hydroxido anionic ligand to the oxygen atoms of one nitrate counterion. A second interaction emerges as the imino group interacts with O(8) and O(8)′ of the second nitrate counter anion, thus forming infinite chains parallel to the *a* crystallographic axis and gives rise to a final 1D lattice.

Compound **3** crystallizes in the monoclinic $P2_1$ space group, with the multiplicity of the general site being two. Crystallographic bond lengths and angles are shown in Table 2 and Table S1. In the asymmetric unit, there is one trinuclear tetracationic $[Co_3(OH)_2(C_6H_{14}NO_2)_2(C_{10}H_8N_2)_3]^{4+}$ complex assembly

Full Paper
doi.org/10.1002/ejic.202000435

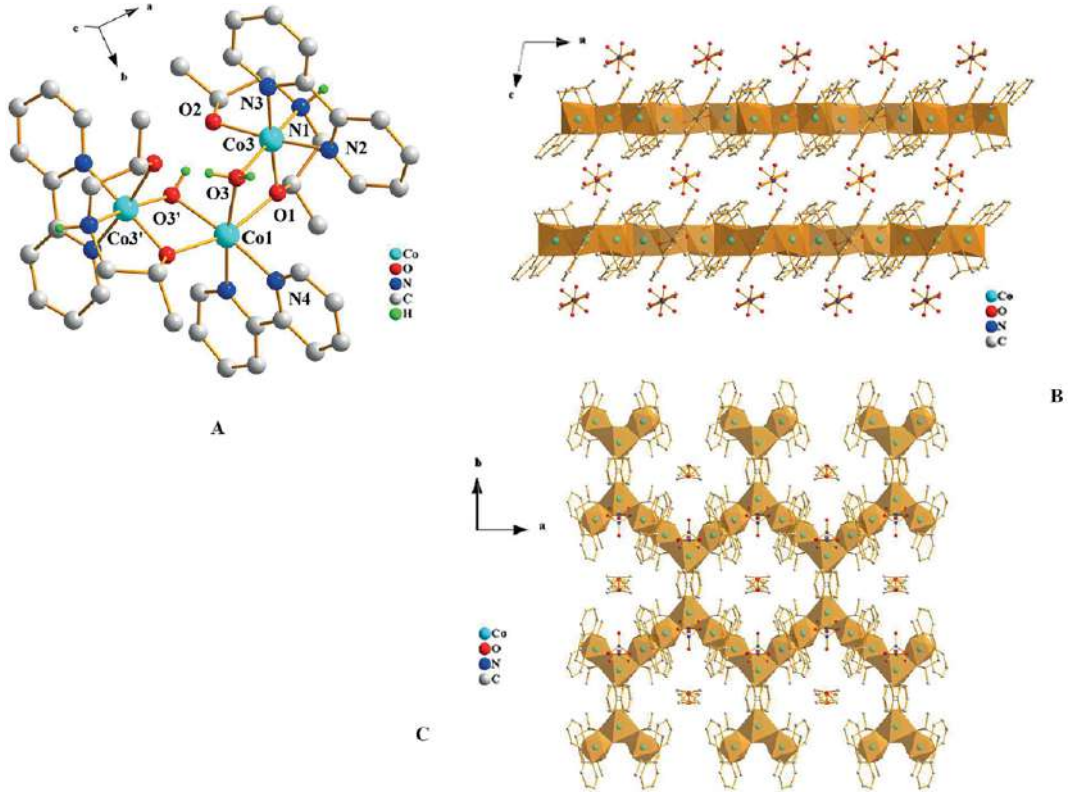

Figure 2. **A.** Diamond plot of cluster assembly $[Co_3(H_2O)(OH)(C_6H_{13}NO_2)_2(C_{10}H_8N_2)_3]^{3+}$ in **2**. **B**. Lattice of **2** in the *ac* plane. **C**. Lattice of **2** in the *ab* plane.

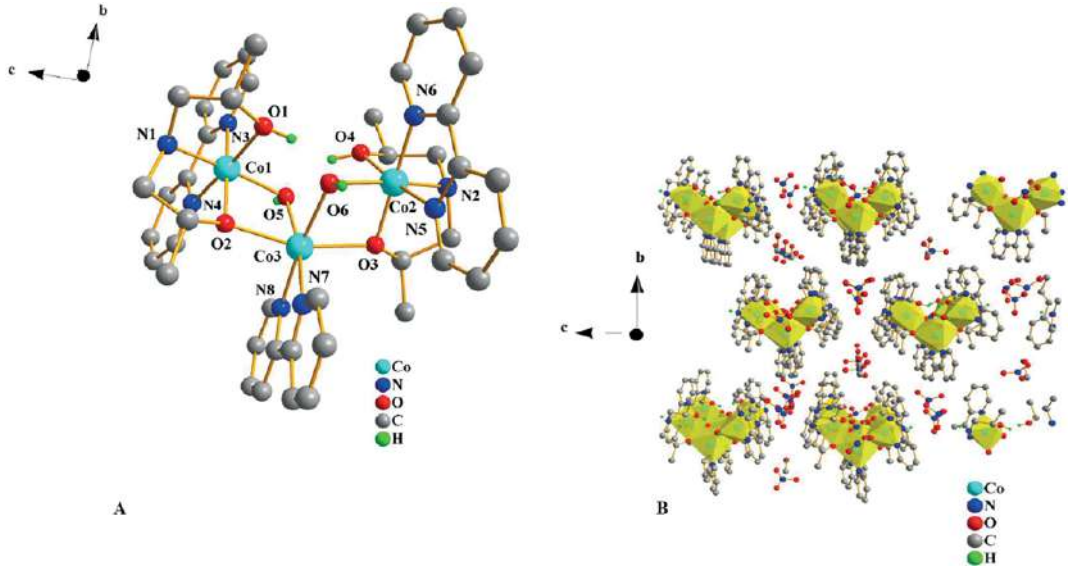

Figure 3. **A.** Diamond plot of cluster assembly $[Co_3(OH)_2(C_6H_{14}NO_2)_2(C_{10}H_8N_2)_3]^{4+}$ in **3**. **B**. Lattice of **3** in the *ac* plane.

(Figure 3**A**), four nitrate counterions and one methanol solvate molecule, all with full occupancy factors, placed on general positions.

The trinuclear mixed ligand-mixed valence cobalt assembly is similar to that in compound **2**, containing one Co(II) (Co(3)) and two Co(III) (Co(1), Co(2)) ions, with metal to metal distances of 3.0609 and 3.0811 Å. The oxidation state assignments for the cobalt centers were supported through BVS calculations, revealing values of 1.921 for Co(II) (Co(3)), and 2.765 and 2.811 for Co(III) (Co(1) and Co(2), respectively). There are three 2,2′-bipy ligands, each coordinated to one metal center through their nitrogen atoms. The difference from the corresponding assembly in **2** is that the two iminodipropanolato ligands, coordinated through their oxygen and nitrogen atoms, are singly deprotonated only on one of the alcoholic groups each. Each protonated alcoholic group is singly coordinated to a Co(III)

Full Paper
doi.org/10.1002/ejic.202000435

center, with each deprotonated oxygen atom bridging Co(III) and Co(II) ions. The octahedral coordination environment is fulfilled with two hydroxido groups, each acting as a double bridge between the Co(III) and Co(II) centers (Figure 3**B**).

Figure 3 **A** portrays the trinuclear tetracationic complex. The Co(III)–O distances vary from 1.880(3) to 1.927(3) Å, with Co(III)–N distances varying from 1.919(4) to 1.944(4) Å, as expected.[37] The Co(II)–O distances vary from 2.089(3) to 2.143(3) Å, with the Co(II)–N distances varying from 2.090(4) to 2.093(4) Å, all typical values for Co(II)–O and Co(II)–N distances.[38,39]

A hydrogen-bonding network emerges as the imino moiety of the iminodipropanolato ligands interacts with one of the lattice nitrate counterions (containing O(7) and O(8)), thus forming chains parallel to the c crystallographic axis. Chains also form as the oxygen atoms of a second lattice nitrate anion interact with the hydroxido anionic ligands of the core assembly containing O(13) and O(14). These chains are parallel to the *a* crystallographic axis. The interactions between the aforementioned described chains form a final rigid 2D crystal lattice, with planes parallel to the a0c crystallographic plane.

Compound **4** crystallizes in the monoclinic *C2/c* space group. Crystallographic bond lengths and angles are shown in Table 2 and Table S1. It contains a mixed valence-mixed ligand tetranuclear complex assembly. The moiety formula $C_{51}H_{56}Co_4N_{11}O_{18}$, projects the main dicationic tetranuclear core $[Co_4(OH)_2(C_6H_{12.5}NO_2)_2(C_{12}H_8N_2)_3(NO_3)]^{2+}$ (Figure 4**A**), two nitrate anions as counterions and three solvate methanol molecules severely disordered over eight positions. The dinuclear cationic assembly consists of four cobalt ions symmetrically generated with respect to the center of symmetry in the mid distance of Co(2)–Co(2)′, both sitting on special positions and being Co(II). The pair of the remaining cobalt ions is comprised of Co(III) ions. The oxidation state assignments for the cobalt centers were supported through BVS calculations, revealing values of 1.960 and 2.006 for Co(II) (Co(2) and Co(3), respectively), and 2.720 for Co(III) (Co(1)). Of the two iminodipropanolato ligands, one is considered as doubly deprotonated and the second one triply deprotonated. This is consistent with the observation that the amine hydrogen was found with an occupancy factor of 0.5, thus rendering the ligand doubly or triply deprotonated over two equivalent symmetrical positions.

Three 1,10-phenanthroline ligands in the assembly are coordinated one to each Co(III) (Co(1), Co(1)′) and to one of the Co(II) (Co(2), Co(3)) centers, in a typical bidentate chelate mode through the two nitrogen atoms. The nitrato ligand is coordinated to the second Co(II) cation in a bidentate chelate fashion through two of the oxygen atoms. In the tetranuclear core, there are also two additional hydroxido anions, both triply bridging one Co(III) and two Co(II) ions though their oxygen atoms.

Figure 4**A** portrays the tetranuclear dicationic complex assembly. The Co(II)–O distances vary from 2.071(3) to 2.126(3) Å, with the Co(II)–N distance found to be 2.102(4) Å, as expected. The Co(III)–O distances vary from 1.887(3) to 1.932(3) Å and the Co(III)–N distances vary from 1.930(4) to 1.976(4) Å, all reflecting typical values for Co(III)-(O,N) distances.[37–39]

Hydrogen-bonding interactions give rise to a complex network connecting the lattice solvent and nitrate anions with the core assembly, thus creating a 3D crystal lattice (Figure 4**B–C**). Specifically, the imido group of the imidodipropanolato ligand and the non-coordinated oxygen atom of the bound nitrato ligand interact with the lattice methanol molecules and the nitrate counter anions, thereby bridging them into a finally emerging 3D network.

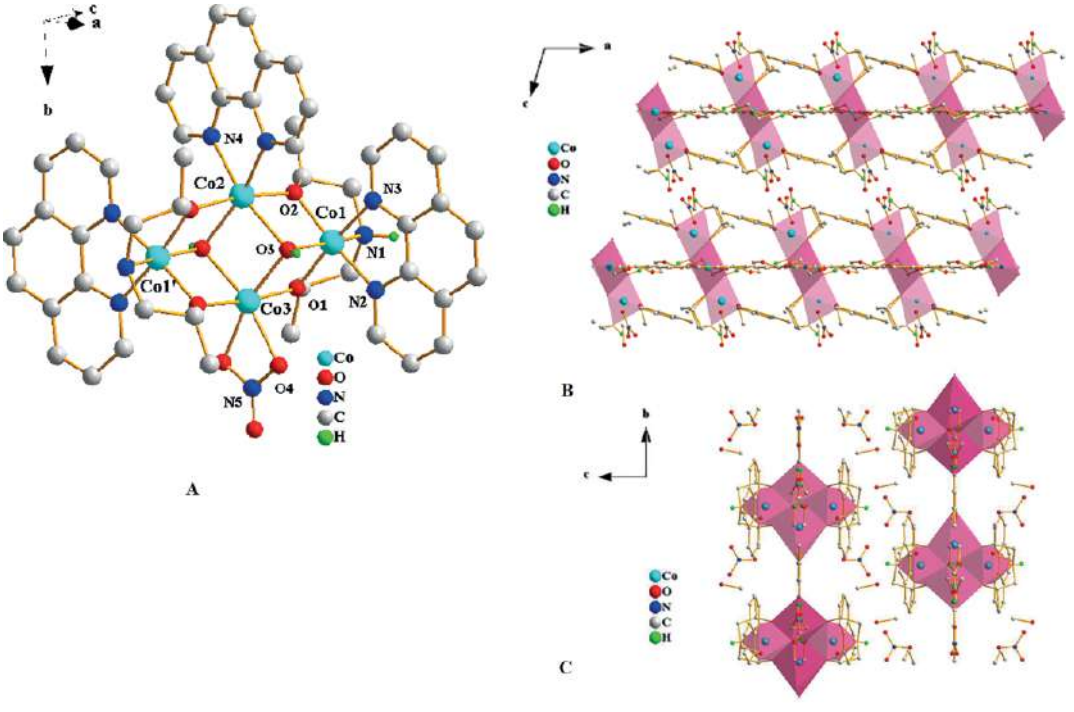

Figure 4. **A.** Diamond plot of cluster assembly $[Co_4(OH)_2(C_6H_{12.5}NO_2)_2(C_{12}H_8N_2)_3(NO_3)]^{2+}$ in **4**. **B**. Lattice of **4** in the *ac* plane. C. Lattice of **4** in the *bc* plane.

Full Paper
doi.org/10.1002/ejic.202000435

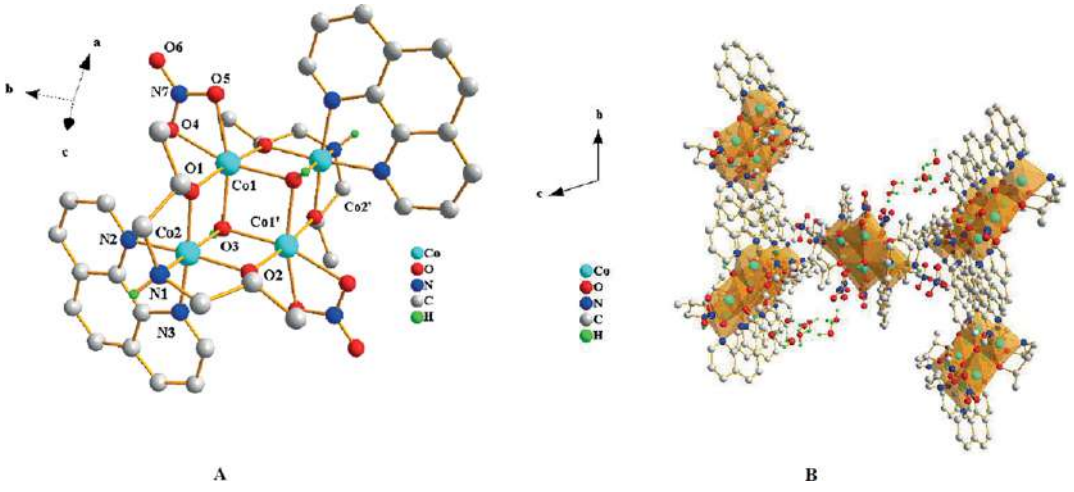

Figure 5. **A.** Diamond plot of cluster assembly $[Co_4(OH)_2(C_6H_{13}NO_2)_2(C_{12}H_8N_2)_2(NO_3)_2]^{2+}$ in **5**. **B**. Lattice of **5** in the *bc* plane.

Compound **5** crystallizes in the triclinic $P\bar{1}$ space group. In the unit cell, there are two slightly different dicationic tetranuclear clusters, four nitrate counterions and totally five disordered water molecules. Each tetranuclear complex $[Co_4(OH)_2(C_6H_{13}NO_2)_2(C_{12}H_8N_2)_2(NO_3)_2]^{2+}$ assembly is comprised of two Co(II) (Co(1), Co(1)′) cations, two Co(III) (Co(2), Co(2)′) cations, two phenanthroline ligands, two iminodipropanol doubly deprotonated anionic ligands, two hydroxido ligands and finally two nitrato ligands. The oxidation state assignments for the cobalt centers in each assembly were supported through BVS calculations, revealing values of 1.972 for Co(II) (Co(1)), and 2.638 for Co(III) (Co(2)).

Each tetranuclear assembly is symmetrically generated from its half, as a result of a center of symmetry residing in the center of the parallelogram formed by the four cobalt ions (Figure 5**A**). The coordination geometry around all cobalt centers is distorted octahedral. Each Co(III) center is surrounded by three nitrogen atoms, coming from the 1,10-phen and the iminodipropanolato ligands. Three oxygen atoms complete the coordination sphere, coming from the iminodipropanolato ligands and the hydroxido anions. Both alcoholato oxygen atoms are doubly-bridging one Co(III) and one Co(II) ions, while each hydroxido anion is triply-bridging one Co(III) and the two Co(II) ions. Each Co(II) ion is surrounded by six oxygen atoms. Four of those come from the iminodipropanolato and the hydroxido ligands as described. The remaining two oxygen atoms on each Co(II) center originate from the two bidentate chelate nitrato anions.

The tetranuclear dicationic cluster is shown in Figure 5**A**. Crystallographic bond lengths and angles are shown in Table 2 and Table S1. The Co(III)–O distances vary from 1.896(2) to 1.956(2) Å, while Co(III)–N distances vary from 1.952(3) to 1.986(3) Å, as expected.[37] The Co(II)–O distances vary from 2.170(3) to 2.053(2) Å, typically encountered values for Co(II)–O distances.[38,39]

Local, only, hydrogen-bonding interactions emerge as the imino group of the iminodipropanolato ligand and the hydroxido anionic ligands interact with the lattice nitrate counter anions (Figure 5**B**). These anions also interact with the lattice water molecules, locally keeping the contents of the unit cell together, but not extending it to any direction.

Compound **6** crystallizes in the orthorhombic *Cccm* space group. Crystallographic bond lengths and angles are shown in Table 2 and Table S1. The formula $C_{10}H_{14}CoN_4O_9$ describes a monomer assembly of a polymeric linear structure reflected in the analytical formula $[Co^{II}(C_{10}H_8N_2)(NO_3)_2(H_2O)_2]_n{\cdot}nH_2O$. In the unit cell, there are four mononuclear units and four lattice water molecules fulfilling the cell void requirements. Each monomeric unit arises from one Co(II) ion, one 4,4′-bipyridine ligand, coordinated through the nitrogen atoms in a unidentate fashion and end-to-end bridging mode to two contiguous metal ions. The oxidation state assignment for the cobalt center was also supported through BVS calculations, revealing a value of 1.714 and 1.961 for Co(II) (in an all-nitrato and aquo ligand environment around the cobalt center, respectively, due to the observed disorder). Also present are two disordered nitrato anions, also coordinated through one of their oxygen atoms, and two bound water molecules, severely disordered and alternating positions with the nitrato anions.

Figure 6**A** displays the mononuclear unit of the polymeric chain observed in lattice of **6** (Figure 6**B–C**). Crystallographic bond lengths and angles are shown in Table 2 and Table S1. The Co(II)–O distances vary from 2.081(5) to 2.155(7) Å, with the Co(II)–N distance being 2.136(5) Å, all distance values as expected.[41,42]

A hydrogen-bonding network emerges as the disordered bound water molecules and nitrate anions interact, thus forming chains parallel to the crystallographic axes *c* and *a*. These chains form a final rigid 2D crystal lattice, with planes parallel to the a0c crystallographic plane.

Hirshfeld Surface Analysis

Hirshfeld surface analysis was carried out on all compound structures investigated synthetically and characterized crystallographically. Mapping was pursued over d_{norm} shape index and curvedness. In the case of compound **1** (Figure 7), Hirshfeld

Full Paper
doi.org/10.1002/ejic.202000435

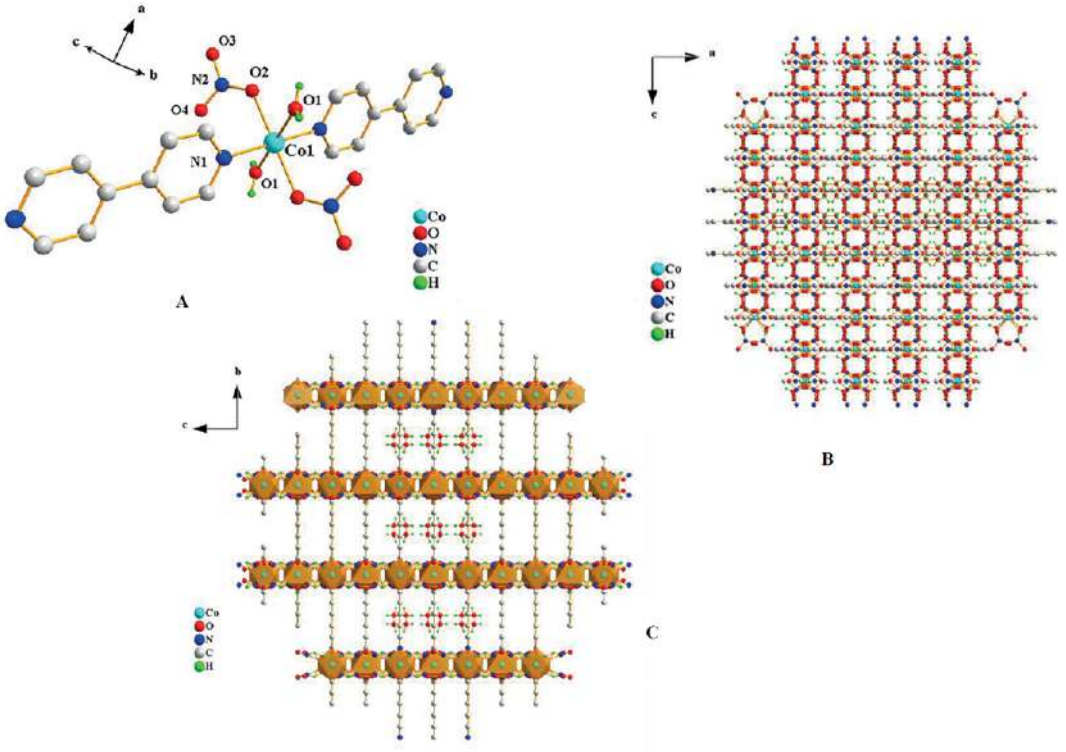

Figure 6. **A.** Diamond plot of mononuclear assembly $[Co(C_{10}H_8N_2)(NO_3)_2(H_2O)_2]$ of the polymeric structure in **6**. **B**. Lattice of **6** in the *ac* plane. **C**. Lattice of **6** in the *bc* plane.

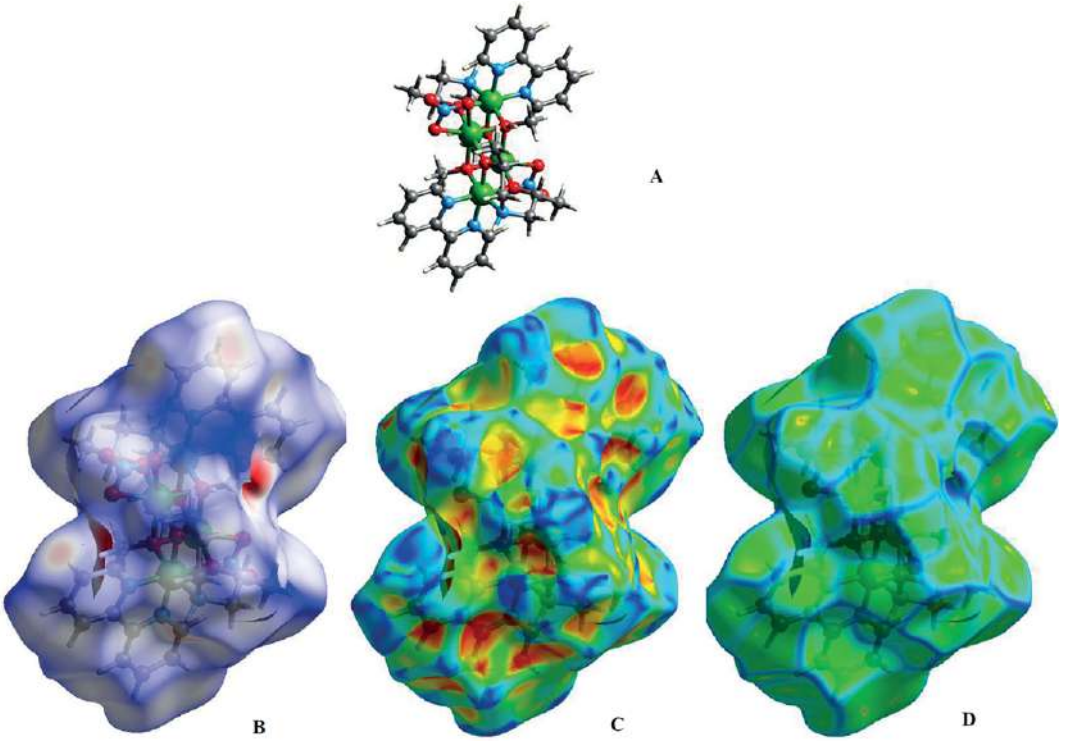

Figure 7. **A.** Crystal explorer plot of **1**. **B.** Hirshfeld surface of **1** mapped over d_{norm}. **C**. Hirshfeld surface of **1** mapped over shape index. **D**. Hirshfeld surface of **1** mapped over curvedness.

surfaces display the most significant interactions involved, with d_{norm} mapping exemplifying strong hydrogen-bond interactions, such as a) O–H···O hydrogen bonding between the cluster cobalt-bound hydroxido moiety and the lattice water oxy-

Full Paper
doi.org/10.1002/ejic.202000435

gen, and b) N–H···O hydrogen bonding between the imino group of the iminodialcoholato ligand and the outer counterion nitrate oxygen. These intermolecular interactions are portrayed in the spots with circular depressions (deep red) visible on the d_{norm} surfaces. The extended intense blue surfaces, close to the bipyridine moiety in the cluster, indicate that abutting clusters in the lattice are quite apart from each other to exhibit interactions between them. The shape index is most sensitive to very subtle changes in surface shape, with the red shaped-spots, represented by concave regions, indicating the presence of atoms involved in weak (C–H···π) interactions and convex blue regions, indicating atoms of the ring of the molecule inside the surfaces. The curvedness is a measure of the shape of the surface area of the complex molecule. The flat areas of the surface reflect low values of curvedness, with sharp curvature regions pertaining to high values of curvedness. They usually tend to partition the surface into patches, indicating interactions between neighboring moieties. This is also the picture depicted in the present cluster. The absence of flat surface patches indicates no extensive planar stacking between neighboring molecules.

The 2D fingerprint plots for **1** (Figure 8) show that intermolecular H···H, O–H···O, and C–H···π interactions are well-defined and stand in complement to the Hirshfeld surfaces. The plots can be deconvoluted to emphasize specific atom pair close contacts,[43] thus delineating distinct contributions from different types of interactions. Two sharp "wing" spikes pointing toward the lower left of the plot are typical C–H···C interactions, of which C–H···π interactions comprise 9.5 % of the total Hirshfeld surfaces for each molecule of **1**. Intertwined emerge H···O/O···H interactions, comprising 29.1 % of the total Hirshfeld surfaces. The relatively broad region exhibiting limitedly resolved spikes in the middle of the plot could be attributed to H···H interactions, comprising 55.9 % of the total Hirshfeld surfaces.

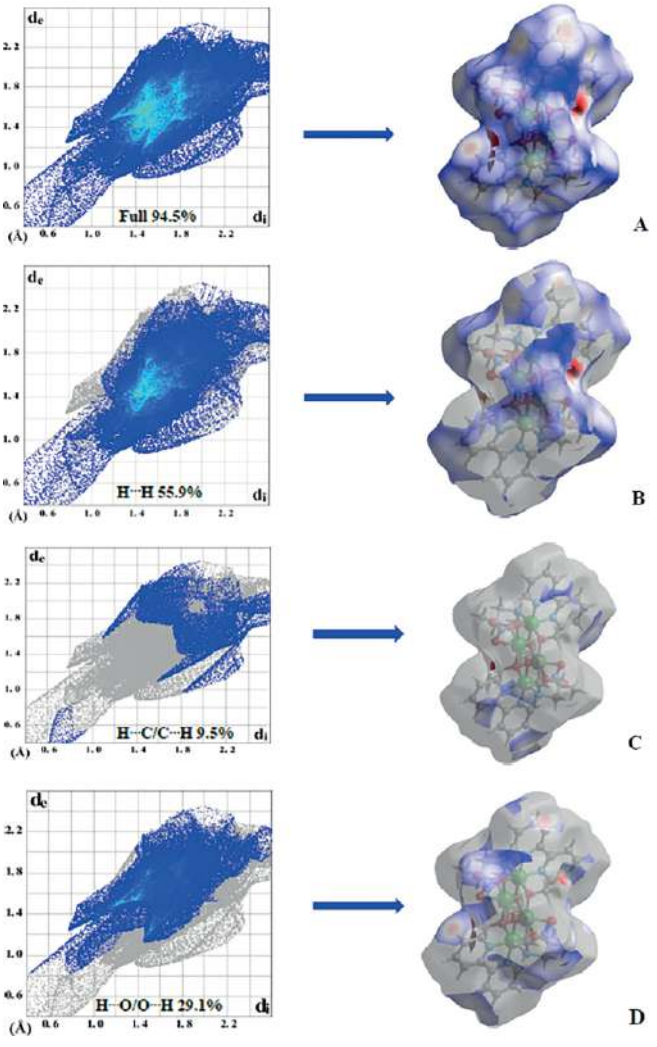

Figure 8. **A.** Full two-dimensional fingerprint plot and the total Hirshfeld area of **1**. **B**. 2D Fingerprint plot of internal vs. external distances between H···H contacts, with the relevant percentage contribution reflected onto the Hirshfeld surface area of **1**. **C**. 2D Fingerprint plot of H···C/C···H contacts, with the relevant percentage contribution reflected onto the Hirshfeld surface area of **1**. **D**. 2D Fingerprint plot of H···O/O···H contacts, with the relevant percentage contribution reflected onto the Hirshfeld surface area of **1**.

In the case of compounds **2** and **3** (Figures S1 and S2, respectively), the derived surface profiles reveal that d_{norm} mapping exemplifies relatively strong hydrogen bond interactions, involving a) O–H···O hydrogen bonding between the cluster cobalt-bound aquo (**2**) and hydroxido (**2**,**3**) moieties on one hand and the counterion nitrate oxygen on the other, and b) N–H···O hydrogen bonding between the imino group of the iminodialcoholato ligand and the outer counterion nitrate oxygen. The intermolecular interactions are shown as circular depressions (deep red) visible on the d_{norm} surfaces. The shape index in **2** shows red shaped-spots, represented by concave regions, indicating the presence of atoms involved in weak (C–H···π) interactions and convex blue regions, indicating atoms of the ring of the molecule inside the surfaces. In **3**, the corresponding picture projects analogous changes with alterations applying to the aforementioned weak interactions and the corresponding participating atoms. Formulation of the differentiated surface in **3** is supported by the lower extent of C–H···π interactions (vide infra) compared to **2**. The curvedness in **2** and **3** is exemplified by flat areas of the surface, reflecting patches indicating interactions between neighboring cluster moieties. The absence of extended flat surfaces indicates no significant planar stacking between neighboring molecules. The 2D fingerprint plots for **2** and **3** (Figure S6 and S7, respectively) show that intermolecular H···H, O–H···O, and C–H···π interactions are well-defined and stand in complement to the Hirshfeld surfaces. It is very important to point out the fact that typical C–H···C interactions (essentially C–H···π interactions) comprise 25.5 % (**2**), with the corresponding figure standing lower at 8.9 % (**3**) of the total Hirshfeld surfaces, thus being in line with the results of the shape index formulations. Interactions of the type H···O/O···H emanating from the mixed asymmetric aquo-hydroxido (**2**) and aquo (**3**) moieties, comprise 28.8 % and 35.5 %, respectively, of the total Hirshfeld surfaces. The relatively broad region, exhibiting limitedly resolved spikes in the middle of the plot, could be attributed to H···H interactions, comprising 39.3 % (**2**) and 48.4 % (**3**) of the total Hirshfeld surfaces.

In the case of compound **4** (Figure S3), d_{norm} mapping exemplifies relatively strong hydrogen bond interactions, involving a)

O–H···O hydrogen bonding between the cluster cobalt-bound hydroxido moiety and the lattice solvent methanol oxygen, b) N–H···O hydrogen bonding between the imino group of the iminodialcoholato ligand and the lattice counterion nitrate oxygen, and c) O···H–O hydrogen bonding between the bound nitrato oxygen and the lattice solvent methanol alcoholic oxygen. The observed intense blue surfaces mostly close to the imino moiety in the cluster indicate that neighboring clusters in the lattice are quite apart from each other to elicit interactions between them. The shape index shows red shaped-spots, represented by concave regions, indicating the presence of atoms involved in weak (C–H···C) interactions. The curvedness is exemplified by the absence of extended flat surfaces, indicating no π···π stacking between neighboring molecules. The 2D fingerprint plot for **4** (Figure S8) shows that intermolecular H···H, O–H···O, and C–H···C interactions are well-defined. The plot points to typical C–H···C interactions comprising 27.0 % of the total Hirshfeld surfaces, with interactions H···O/O···H standing at 29.5 % of the total Hirshfeld surfaces. The observed spike pattern in the fingerprint plot indicates the fact that one molecule acts as a donor ($d_e > d_i$) and the other one as an acceptor ($d_e < d_i$). The relatively broad region exhibiting limitedly resolved spikes in the middle of the plot could be attributed to H···H interactions, comprising 35.3 % of the total Hirshfeld surfaces.

In the case of compound **5** (Figure S4), d_{norm} mapping exhibits its relatively strong hydrogen bond interactions, involving a) O–H···O hydrogen bonding between the cluster cobalt-bound hydroxido moiety and the lattice water oxygen, in one of the two molecules in the unit cell, and the hydroxido moiety on the second molecule and the counterion nitrate oxygen, and b) N–H···O hydrogen bonding between the imino group of the iminodialcoholato ligand and the lattice counterion nitrate oxygen. The shape index shows red shaped-spots, represented by concave regions, indicating the presence of atoms involved in weak (C–H···π) interactions between neighboring molecules. The curvedness is exemplified by the presence of extended flat surfaces, indicating π···π stacking between neighboring molecules. The 2D fingerprint plot for **5** (Figure S9) shows that intermolecular H···H, O–H···O, and C–H···C interactions are well-defined. The plot points to typical C–H···π interactions comprising 11.7 % of the total Hirshfeld surfaces, with H···O/O···H interactions standing at 37.5 % of the total Hirshfeld surfaces. The relatively broad region exhibiting limitedly resolved spikes in the middle of the plot could be attributed to H···H interactions, comprising 42.2 % of the total Hirshfeld surfaces.

In the case of polymeric compound **6** (Figure S5), d_{norm} mapping exhibits relatively strong hydrogen bond interactions, involving O–H···O hydrogen bonding between the cluster cobalt-bound aquo/nitrato moiety and the corresponding nitrato/aquo oxygen of a neighboring molecule in the unit cell. The shape index shows red shaped-spots, represented by concave regions, indicating the presence of atoms involved in weak (N···H and C–H···C) interactions between neighboring molecules. The curvedness is exemplified by the presence of extended flat surfaces confound by not so starkly intense blue outlines, indicating no π···π stacking and weak C–H···C interactions between neighboring molecules. The 2D fingerprint plot for **6** (Figure S10) shows that intermolecular H···H, O–H···O, N···H–O, C···C and C–H···C interactions are well-defined. The plot points to C–H···C interactions comprising 13.6 %, N···H–O 4.1 %, H···O/O···H interactions standing at 37.3 %, and C···C interaction reflecting 9.1 % of the total Hirshfeld surfaces. The relatively broad region in the middle of the plot could be attributed to H···H interactions, comprising 20.5 % of the total Hirshfeld surfaces.

FT-IR Spectroscopy

The FT-IR spectra of compounds **1–6** in KBr exhibit shifted bands related to ν(C-N) bond vibrations in 2,2′-bipy, 1,10-phen and 4,4′-bipy, thus indicating bond formation to metal ions. Specifically, strong ν(C-N) bond vibrations of 2,2′-bipy emerged[44] at 1631 cm^{-1} for **1**, and 1612 cm^{-1} for **2** and **3**. In compounds **4** and **5**, strong ν(C-N) bond vibrations were observed to be shifted to 1387 cm^{-1} and 1429 cm^{-1}, respectively, compared to the free 1,10-phen ligand (1419 cm^{-1}).[45] In **6**, the ν(C-N) bond vibration of 4,4′-bipy[46] appeared at 1603 cm^{-1}. Furthermore, the bands in the range from 3050 to 2400 cm^{-1} reveal the presence of the chelating ligand bound to the metal ion centers. Frequencies in the range 420–480 cm^{-1} for compounds **1–5** and at 482 cm^{-1} for **6** suggest the presence of both the aromatic binder ligand,[47,48] and Co–N bonds in **1–6**, thus indicating changes in the vibrational pattern of the ligand upon metal coordination. The NO_3 group, depending on the coordination mode, exhibited absorption features at 1387 cm^{-1} for **1**, 1385 cm^{-1} for **4**, and 1385 cm^{-1} for **5**, when bound in a bidentate fashion, and at 1382 cm^{-1} for **6** when anchored to the metal center through a monodentate mode. Also, the presence of strong bands above 3400 cm^{-1} signifies the presence of O-H stretches. Ligand coordination to the cobalt centers in compounds **1–5** is reflected onto Co–O vibrations appearing in the range 500–604 cm^{-1},[49] higher than Co–N vibrations.

UV/Visible Studies

The UV/Vis spectra of **1**, **4**, **5**, and **6** were recorded in methanol (Figure 9, S11–S13). All spectra exhibit a broad band in the low energy region, at 524 nm (**1**), 530 nm (**4**), 528 nm (**5**), and 512 nm (**6**), consistent with the presence of d-d transitions and

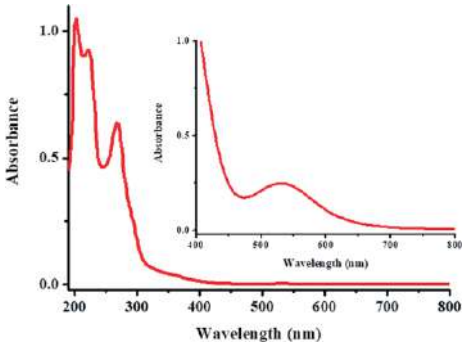

Figure 9. UV/Visible spectrum of compound **4** in methanol (1.0×10^{-5} M). **Inset:** spectrum of **4** (8.0×10^{-4} M) in the low energy region, showing the d-d transition.

commensurate with the presence of the coordinated ionic cobalt centers in the respective cluster assemblies. Beyond that feature, compound **1**, the only one examined and containing 2,2′-bipy in the coordination sphere of cobalt in the specific cluster, exhibits five absorption features at higher energies, all attributable to LMCT[50–52] transitions (Table 3). In contrast to that, the remaining species **4**, **5,** and **6**, not containing 2,2′-bipy, exhibit four ostensible absorptions at higher energies, all attributable to LMCT transitions (Figure 9, Table 3).

Table 3. UV/Visible spectral parameters of electronic spectra of compounds **1**, **4**, **5**, and **6** in methanol.

Compound	Wavelength (nm)	Molecular absorption coefficient (ε, M^{-1} cm^{-1})
1	206	54966
	238	39643
	302	16440
	312	16482
	ca. 358 (sh)	ca. 2503
	524	272
4	204	97354
	226	81680
	268	60813
	ca. 360 (sh)	ca. 4051
	530	313
5	202	83215
	222	72569
	270	47596
	ca. 358 (sh)	ca. 3702
	528	273
6	200	31831
	236	12982
	ca. 268 (sh)	ca. 5339
	ca. 462 (sh)	ca. 9
	512	12

Luminescence Studies

The solid-state spectra of **1**, **4**, **5**, and **6**, along with those of 2,2′-bipy, 1,10-phen, and 4,4′-bipy, were recorded at room temperature. The spectroscopic data reveal that 1,1′-iminodi-2-propanol does not possess any luminescence. In contrast to that, free 2,2′-bipy, 1,10-phen, and 4,4′-bipy exhibit a strong band at 388 nm (λ_{ex} 322 nm), a pattern of three features with the strongest being at 417 (λ_{ex} 368 nm), and a strong band at 358 nm (λ_{ex} 323 nm), respectively. The emission spectra of **1** (Figure 10) show well-resolved features at 453 and 470 nm (λ_{ex} 357 nm). The corresponding spectra of **4** exhibit well-resolved features at 453 and 471 (λ_{ex} 327 nm), with the spectra of **5** showing two well-resolved absorptions at 454 and 472 (λ_{ex} 325 nm). Finally, the emission spectra of **6** show a pattern of less well-resolved features including those at 402, 453 and 471 (λ_{ex} 290 nm). The observed luminescence spectra, in all cases of described compounds, could be attributed to ligand-to-metal-charge-transfer (LMCT) processes.[52–55] Ostensibly, the electronic features observed in the luminescence spectra arise as a result of the presence of the aromatic ligands in the coordination sphere of cobalt in the respective complex assemblies. As a result of the spectroscopic signatures observed in the compounds studied (Figures S14–S16), it appears that there is a) strong quenching of the luminescence signal of the aromatic ligand upon coordination to cobalt, compared to the signal of the free ligand, and b) a significant shift of the emission features in the respective compounds to lower energies. In view of the fact that the iminodialcoholic ligand does not exhibit any luminescence at room temperature, the possibility arises that the new ternary compounds **1**, **4**, **5,** and **6** could serve as potential electronic switches.

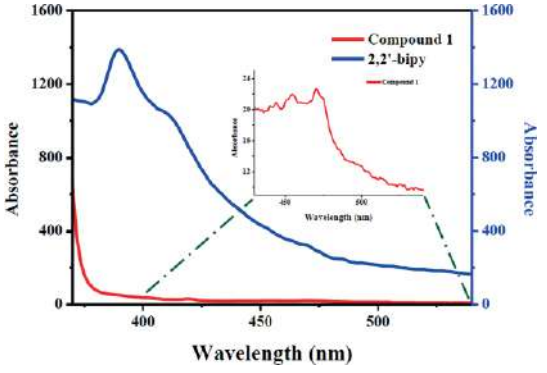

Figure 10. Luminescence spectrum of compound **1** and 2,2′-bipy in the solid state. **Inset:** blow up of spectrum of **1** in the visible region.

Cyclic Voltammetry

Electrochemical measurements for compounds **1**, **4–6** were recorded in methanol, at various scan rates (100–400 mV/s), in the presence of Bu_4NClO_4 as a supporting electrolyte. A Pt electrode was used as working electrode and an $Ag/AgNO_3$ electrode served as a reference electrode. The cyclic voltammogram of **1** exhibits a cathodic wave (Figure S17) at E_{pc}= –1.02 V and an anodic wave at E_{pa} = –0.64 V. The cyclic voltammograms of **4** and **5** show cathodic waves (Figures S18–S19) at E_{pc} = –1.01 V, and –1.01 V, and anodic waves at E_{pa} = –0.56 V and –0.60 V, respectively. In the case of compound **6**, the observed waves are a cathodic wave (Figure S20) at E_{pc}= –1.01 V and an anodic wave at E_{pa} = –0.71 mV. Wide scans in the –2.0 to +2.0 Volt range as well as narrower range scans were investigated on all systems mentioned in both scan directions. The observed electrochemical profile for all compounds tested is ill-defined and consistent with irreversible multi-electron electron redox processes, involving the cobalt and ligand participants in the mononuclear and oligonuclear compounds.

Magnetic Susceptibility Studies

The temperature dependence of susceptibility for compounds **1**, **4**, and **5** was measured under external magnetic fields of 0.1 and 1.0 Tesla, in the temperature range 1.8–320 K. The relevant χ_MT vs. T graphs are shown in Figure 11, Figure 12, and Figure 13. The χ_MT values at 300 K for compounds **1**, **4**, and **5** are ca. 6.5, 6.6, and 6.8 emu mol^{-1} K, respectively, close to the value expected for two non-interacting Co(II) ions with S = 3/2 and g = 2.63, 2.65, and 2.70. The high-temperature behavior is consistent with the presence of a significant orbital contribution

Full Paper
doi.org/10.1002/ejic.202000435

due to the anisotropic nature of the Co(II) ion.[56–58] The $\chi_M T$ values remain essentially stable until 60 K and then increase more steeply to a maximum value of 8.5, 8.6, and 7.8 emu mol^{-1} K, respectively at 10 K, with an ensuing abrupt decrease to the value of 6.7, 6.9, and 5.8 emu mol^{-1} K at 2 K, respectively. The increase of magnetic susceptibility is due to a ferromagnetic interaction between the Co(II) ions, with the abrupt low temperature decrease of the susceptibility data due to zero field/intermolecular interactions. Field-dependent magnetization data are shown as insets in Figure 11, Figure 12, and Figure 13.

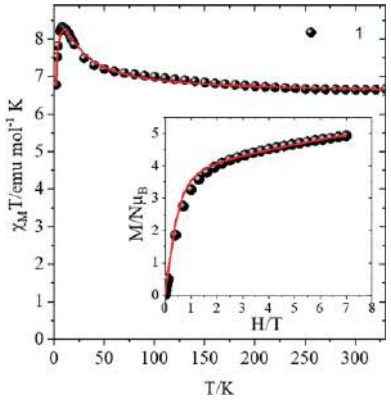

Figure 11. Temperature dependence of the susceptibility data of compound **1** in the form of $\chi_M T$/per 2Co(II) ions vs. *T* at 0.1 T. The solid line is the theoretical curve according to the Hamiltonian equation (1) (see text for details). In the inset, the magnetization data are shown in the form of reduced magnetization, $M/N\mu_B$, in the field range 0–7 T and at T 2 K. The solid line is the theoretical curve according to the Hamiltonian equation (1) (see text for details).

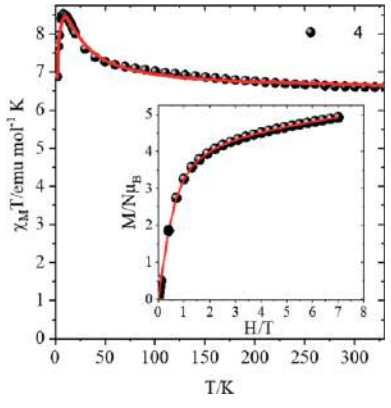

Figure 12. Temperature dependence of the susceptibility data of compound **4** in the form of $\chi_M T$/per 2Co(II) ions vs. *T* at 0.1 T. The solid line is the theoretical curve according to the Hamiltonian equation (1) (see text for details). In the inset, the magnetization data are shown in the form of reduced magnetization, $M/N\mu_B$, in the field range 0–7 T and at T 2 K. The solid line is the theoretical curve according to the Hamiltonian equation (1) (see text for details).

Temperature dependence of the susceptibility data of compound **1** in the form of $\chi_M T$/per 2Co(II) ions vs. *T* at 0.1 T. The solid line is the theoretical curve according to the Hamiltonian equation (1) (see text for details). In the inset, the magnetization data are shown in the form of reduced magnetization, $M/N\mu_B$, in the field range 0–7 T and at T 2 K. The solid line is the

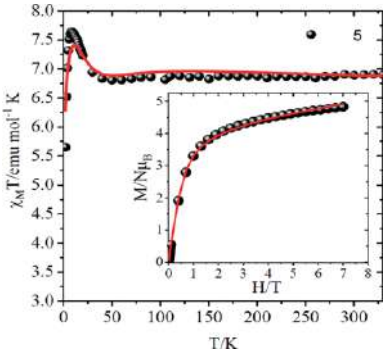

Figure 13. Temperature dependence of the susceptibility data of compound **5** in the form of $\chi_M T$/per 2Co(II) ions vs. *T* at 0.1 T. The solid line is the theoretical curve according to the Hamiltonian equation (1) (see text for details). In the inset, the magnetization data are shown in the form of reduced magnetization, $M/N\mu_B$, in the field range 0–7 T and at T 2 K. Solid line is the theoretical curve according to the Hamiltonian equation (1) (see text for details).

theoretical curve according to the Hamiltonian equation (1) (see text for details).

The employed fitting model for the magnetization and susceptibility data is shown in equation (1).[59] The terms in the summation represent the Zeeman, single ion D anisotropy and mean field correction of each magnetic ion within a single molecule. The axial and transverse Zero Field Splitting (ZFS) parameters D and E are defined by the D tensor as: $D = 3/2D_{zz}$ and $E = 1/2(D_{xx} - D_{yy})$, while the *zJ* term is added to the theoretical model to describe possible intermolecular interactions due to the extended hydrogen network.

$$\hat{H} = J\hat{S}_1 \cdot \hat{S}_2 + \sum_{i=1,2}\left(\mu_B \boldsymbol{B} \cdot \boldsymbol{g_i} \cdot \hat{S}_i + \hat{S}_i \cdot \boldsymbol{D_i} \cdot \hat{S}_i - zJS_{iz}\langle S_{iz}\rangle\right) \quad (1)$$

In order to overcome the over-parameterization of the theoretical model, both susceptibility and magnetization data were fitted through the same equation and the results are shown in Table 4. The theoretical curves are shown as a solid line in the same figures. From the susceptibility data, it was found that exchange interactions for the **1, 4** are close to 2 cm^{-1}, while a

Table 4. Fitting results of susceptibility and magnetization data according to the Hamiltonian formalism of Equation (1) and (2).

Compound	Susceptibility fitting values	Magnetization fitting values
1	J_{12} = 1.7 cm^{-1} g_i = 2.64[a] (D_i,E_i) = (9.8, 1.1)[a] cm^{-1}	J = 0.9 cm^{-1} g_i = 2.61 (D_i,E_i) = (18.0, 5.0) cm^{-1}
4	J = 1.8 cm^{-1} g_i = 2.63 (D_i,E_i) = (9.2, 1.0) cm^{-1}	J = 1.0 cm^{-1} g_i = 2.5 (D_i,E_i) = (24.0, 5.0) cm^{-1}
5	J = 1.0 cm^{-1} g_i = 2.65 (D_i,E_i) = (7.3, 1.1) cm^{-1} zJ = –0.02 cm^{-1}	J = 0.6 cm^{-1} g_i = 2.5 (D_i,E_i) = (22, 0.5) cm^{-1}
6	g = 2.6, (D,E) = (54.6, 6.1) cm^{-1} g = 2.6, (D,E) = (67.6, 5.1) cm^{-1}, zJ = –0.03 cm^{-1}	

[a] i = 1–2.

weaker ferromagnetic interaction close to 1 cm^{-1} is calculated for compound **5.** Moreover, for the latter compound, an antiferromagnetic intermolecular interaction was observed due to the extended hydrogen network. It was not possible to derive a value for the mean field correction in the case of the other two compounds, due to correlation issues with the D parameter during the fitting process. The ZFS parameters are close to the values expected for octahedral Co(II) ions.[60] From the magnetization data, the values of the exchange interactions were underestimated, with the D and E parameters being overestimated, possibly because at 2 K intermolecular interactions influence the behavior of the magnetization data.

The magnetic behavior of compound **6** is shown in Figure 14. The $\chi_M T$ values of compound **6** decrease smoothly from 3.2 emu mol^{-1} K at 300 K to 2.6 emu mol^{-1} K at 100 K and then more steeply to a minimum value of 1.6 emu mol^{-1} K at 2 K. Field-dependent magnetization data are shown as inset in the same Figure 14.

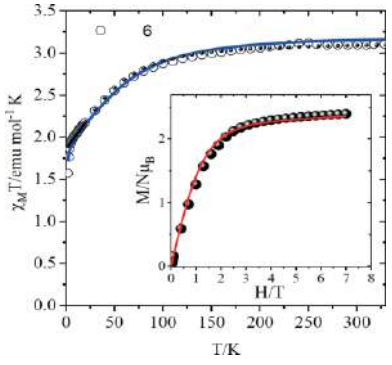

Figure 14. Temperature dependence of the susceptibility data of compound **6** in the form of $\chi_M T$/per Co(II) ions vs. *T* at 0.1 T. The solid line and solid spheres are the theoretical curves according to the Hamiltonian equation (2) with and without the incorporation of a mean field correct, *zJ*, respectively (see text for details). In the inset, the magnetization data are shown in the form of reduced magnetization, M/Nμ_B, in the field range 0–7 T and at T 2 K. The solid line is the theoretical curve according to the Hamiltonian equation (2) (see text for details).

This behavior is consistent with the presence of a significant orbital contribution, with the employed fitting model for the susceptibility and magnetization data shown in Equation 2. In order to simulate the magnetic behavior of this 1D chain, we used the approximation of a dimer model, with a mean field correction for the weak intrachain interactions. The model[59] takes into account a) both the axial and transverse ZFS parameters D and E, b) an isotropic *g* value, and c) the mean field correction due to the intermolecular interactions, with the results shown in Table 4. Two different sets of parameters were obtained from the simultaneous fit of the susceptibility and magnetization data. In the case of negligible intermolecular interaction (*zJ* = 0), the theoretical curve is shown as solid spheres in the same figure, whereas a solid line reflects the case of nonzero intermolecular interactions (zJ = –0.03 cm^{-1}).

$$\hat{H} = \mu_B \boldsymbol{B} \cdot \boldsymbol{g_i} \cdot \hat{S}_i + \hat{S}_i \cdot \boldsymbol{D_i} \cdot \hat{S}_i - zJS_z\langle S_z\rangle \qquad (2)$$

In all cases, the sign of the D and E was not resolved from the magnetic measurements, while introduction of an axial symmetry to the g-parameter ($g_\perp$, $g_\parallel$) did not improve the fitting results.

Electron Paramagnetic Resonance (EPR) Studies

X-band powder and solution EPR measurements were carried out on samples of compounds **1**, **4**, **5**, and **6** and are shown in Figure 15 and Figure S21. Signals were observed only below 50 K, as a consequence of the fast spin-lattice relaxation time of high-spin Co(II). The broadening effect is related to the conversion of the g-strain into B-strain through the equation

$$\Delta B = -\left(\frac{h\nu}{\mu_B}\right)\left(\frac{\Delta g}{g^2}\right)$$

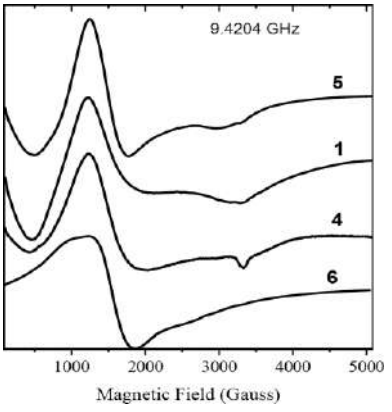

Figure 15. Powder X-band EPR spectra of compounds **1**, **4**, **5**, and **6** at 4 K.

where the parameters have their usual meaning.[58] According to this effect, the largest and smallest g-values of the powder spectra have field widths that differ by an order of magnitude, thereby rationalizing the broad high-field features of the spectrum. In order to investigate the existence of a weak interaction between the Co(II) centers in complexes **1**, **4**, and **5**, X-band powder EPR experiments were carried out in the temperature range 4–40 K. The powder spectra at 4 K are shown in Figure 15. The *g* values obtained from the powder EPR spectra show large variations in the range 20.0–2.0, thereby indicating a ferromagnetic exchange interaction between the Co(II) ions. In the case of compound **6**, a derivative appears centered at ca. g = 5.3, which is a clear indication of a high spin Co(II) monomer.[59] The frozen solutions of compounds **1**, **4**, **5**, and **6** (Figure S21) gave the same spectrum with a derivative centered at ca. g = 5.3, clearly indicating that the compounds do not retain their structure in solution.

Discussion

Synthetic Challenges in Ternary Crystalline Phases

It is often perplexing to envision ternary systems of metal ions with binary and ternary partners providing well-defined products of discrete nuclearity and composition. The present work employed a specific metal ion, i.e. Co(II), and an iminodialcohol system as the binary basis of reactivity in alcoholic media. Al-

Full Paper
doi.org/10.1002/ejic.202000435

beit complex in its inception and implementation, the specific metal-organic system has been investigated synthetically from the point of view of a) composition, with the ternary partners being aromatic chelators, such as 2,2′-bipy and 1,10-phen, b) molecular stoichiometry, and c) temperature of the reaction, all in the presence of a defined solvent system (methanol). Careful investigation of the reactivity system employed initially methanol and a series of dual reaction conditions (4 and 25°C), through which discrete crystalline materials were isolated and crystallographically characterized. More specifically, the molecular stoichiometry Co(II):iminodipropanol:(N,N′-aromatic chelator) was varied from 1:1:1 to 2:1:1 in a temperature-dependent fashion, with the arising materials isolated and examined spectroscopically and crystallographically. Materials **1–5** exemplify the impact of the distinct nature of reaction conditions, leading to the isolation of crystalline materials with variable yields.

Specifically, the behavior observed in the ternary Co(II):iminodipropanol:(2,2′-bipy) system in methanol reveals that for the 2:1:1 stoichiometry at both 4 and 25°C, the compound isolated exclusively is **1**. In contrast to that, the 1:1:1 system exhibits a different behavior, with the 25°C system leading to the isolation of compound **1**. In the case of the system at 4°C, what is consistently isolated from the same system is a mixture of **2** and **3**. This reproducible behavior, having been examined at least ten times, is subject to no change toward one compound or another (for **2** and **3**) regardless of the number of efforts made and condition changes employed. Confirmation of the identity of the two components, concurrently arising through the system, came from X-ray crystallography and FT-IR spectroscopy.

Maintaining the identity of the system and changing the N,N′-aromatic chelator from 2,2′-bipy to 1,10-phen, leads to a totally different behavior. Specifically, for the ternary Co(II):iminodipropanol:(1,10-phen) system with a 1:1:1 molecular stoichiometry, both the 4°C and 25°C attempts led to the isolation of the same material **4**. For the same system, yet different molecular stoichiometry 2:1:1, reactivity led to a different compound **5**, the same for the two temperatures investigated.

Albeit not unexpectedly, the same basic Co(II):iminodipropanol system involving the aromatic binder 4,4′-bipy, instead of 2,2′-bipy or 1,10-phen, with a 2:1:1 molecular stoichiometry, leads to the isolation of pure compound **6** at 4°C. In all cases of ternary systems studied, the arising crystalline phases (Table 5) were fully characterized crystallographically, followed by in-depth physicochemical characterization (FT-IR, UV/Visible, Luminescence, cyclic voltammetry, magnetic susceptibility, and EPR). The collective data support a well-defined temperature and molecular stoichiometry profile of ternary Co(II,III):iminodipropanol:(N,N′-aromatic chelator) systems linked to discrete nuclearity ternary clusters bearing distinctly defined properties (vide infra).

Chemical Reactivity Insights

The successful isolation of six compounds of the investigated ternary systems, based on Co(II) and iminodipropanol in methanol, reveals that there is a specific trend in the chemistry of the reagents employed, when it comes to the assembly of species isolated in crystalline form and in a defined phase. The salient reactivity factors examined during the undertaken synthetic investigation emerged as reactivity indices-markers linked to the identity of the compounds isolated. From temperature-dependent reactions of a given stoichiometry, it was observed that compounds of specific composition, nuclearity and metal oxidation state (Co(II) and Co(III)) arose. In all cases studied, crystallographic as well as Bond Valence Sum calculations were in line with the observed oxidation states of the cobalt centers in the requisite assemblies (vide infra). Interwoven with the temperature dependence was the molecular stoichiometry of the ternary partners participating in the reactions examined. At the first level of inquiry, molecular stoichiometry was linked to a temperature-dependent identity of the compounds isolated, with the aromatic chelator intervening to generate ternary species, with occasional structural intrusion of alcoholato or hydroxido bridges as well as water molecules serving as bridges.

Ligand-Based Reactivity toward Divalent Metal Ions

The ligand iminodipropanol is a potentially tridentate ligand, owing to the presence of two alcohol moieties and an sp^3 nitrogen moiety. In that capacity, the ligand in all cases was bound to the participating cobalt ions in a tridentate fashion. It appears that a) the deprotonation state of the bound ligand was either 2- or 3- or both at the same time in the same metal-

Table 5. Global summary of chemical reactivity in the investigated Co(II):iminodialcohol:(N,N′-aromatic chelator) systems.

No.	Reactants	Molecular stoichiometry	Temperature	Compound
1	Co(II):limino:2,2′-bipy Co(II):limino:2,2′-bipy Co(II):limino:2,2′-bipy	1:1:1 2:1:1 2:1:1	25°C 4°C 25°C	$[Co^{II}_2Co^{III}_2(OH)(CH_3O)(C_6H_{12.5}NO_2)_2(C_{10}H_8N_2)_2(NO_3)_2](NO_3)\cdot 3CH_3OH\cdot H_2O$
2	Co(II):limino:2,2′-bipy	1:1:1	4°C	$[Co^{II}Co^{III}_2(H_2O)(OH)(C_6H_{13}NO_2)_2(C_{10}H_8N_2)_3](NO_3)_3\cdot 2CH_3OH$
3				$[Co^{II}Co^{III}_2(OH)_2(C_6H_{14}NO_2)_2(C_{10}H_8N_2)_3](NO_3)_4\cdot CH_3OH$
4	Co(II):limino:1,10-phen Co(II):limino:1,10-phen	1:1:1 1:1:1	4°C 25°C	$[Co^{II}_2Co^{III}_2(OH)_2(C_6H_{12.5}NO_2)_2(C_{12}H_8N_2)_3(NO_3)](NO_3)_2\cdot 3CH_3OH$
5	Co(II):limino:1,10-phen Co(II):limino:1,10-phen	2:1:1 2:1:1	4°C 25°C	$[Co^{II}_2Co^{III}_2(OH)_2(C_6H_{13}NO_2)_2(C_{12}H_8N_2)_2(NO_3)_2](NO_3)_2\cdot 2.5H_2O$
6	Co(II):limino:4,4′-bipy	2:1:1	4°C	$[Co^{II}(C_{10}H_8N_2)(NO_3)_2(H_2O)_2]_n\cdot nH_2O$

organic assembly, b) the ligand was either attached to a single metal center or acted, through one of its oxygen terminals, as a bridge between neighboring metal centers, c) binding in a tridentate fashion was consistent with the potential bite of the terminal anchors, regardless of the number and oxidation state of the cobalt ions present in the assembled clusters. Irrespective of the nuclearity of the assembly achieved, isolated and characterized crystallographically, the ligand always bound the metal centers through both the sp^3 nitrogen and the two alcoholato terminals. These were also the potential sites of deprotonation of the iminodipropanol ligand.

Structural Speciation in the Presence of Aromatic Chelators

As a result of the aforementioned chemical reactivity in the ternary Co(II):iminodipropanol:(2,2′-bipy) system, temperature emerges as a deciding factor in the determination of the composition of the isolated tetranuclear cluster **1**. Regardless of the employed molecular stoichiometry (1:1:1 or 2:1:1), the consistently isolated crystalline material **1** at two different temperatures (4 and 25°C for the 2:1:1 and 25°C for the 1:1:1) possesses a specific composition, amounting to a Co_4O_6 assembly consisting of two fused cuboids, each missing an apex (diametrically opposed sites of the entire assembly). Interestingly, two of the O-containing non-ligand-associated apices are heteroleptic (OH^- and CH_3O^-), thereby introducing significant asymmetry in the entire cluster assembly. Albeit heterologous, the two apical ligands reflect a characteristic tetrahedrality in the specific cluster sites. The unique assembly is further supported by two N,N′-aromatic chelating bipyridines bound to cobalt centers on the opposite far sites of the cluster, with the intervening closer cobalt pair sites bound to nitrates. In this respect, the discrete contribution of the nitrates originating in the starting Co(II) reagent and the ternary aromatic chelators is clearly exemplified in the ostensibly emerging behavior of that system's reactivity. It is quite surprising that the latter stoichiometry (1:1:1) at 4°C leads to a totally different behavior tantamount to two different products; compounds **2** and **3**. The molecular composition of **2** and **3**, reveals that a) the tetranuclear cluster in **1** no longer appears as a product. In fact, a trinuclear complex emerges instead of a tetranuclear cluster in **1**, b) one of the bridging ligands (CH_3O^-) has been replaced by a water molecule (**2**) or an OH^- group (**3**), c) the ligand bound to the cobalt centers is either doubly deprotonated (**2**) or singly deprotonated (**3**), d) nitrates no longer exist as bound ligands to the cobalt centers. They have been replaced by 2,2′-bipy ligands, thereby raising the total number of 2,2′-bipy ligands in each complex to three, and e) the number of counterion nitrates has been raised, thus attesting to changes in the number of cobalt centers in each complex as well as the assumed oxidation states of those sites (vide infra). The only common feature in all three species **1–3** is the presence of methanol and/or water molecules in the lattice of the compounds in question.

Undoubtedly, the temperature stands as a factor in guiding the structural speciation of the species arising in the reaction mixture investigated, thus confirming the wealth of structures present in such mixtures and concurrently the possibility of using that physical property to guide the system toward one or the other direction, leading to discretely identifiable species.

A more logical, still interwoven, interdependability of temperature and molecular stoichiometry emerges in the case of the ternary system containing 1,10-phen. There, temperature takes the back seat, with the molecular stoichiometry being the decisive factor in the isolation of discrete complex species. Specifically, in the case of the 1:1:1 vs. 2:1:1 stoichiometry, regardless of the temperature variation (4 or 25°C), the species isolated is a tetranuclear cluster **4** vs. a tetranuclear cluster **5**. In that cluster (**4**), a) the bridging ligands in the two cuboids are OH^- groups, a feature also retained in cluster **5**, b) the two bound iminodipropanol ligands are doubly and triply-deprotonated in **4**, whereas doubly deprotonated in **5**, c) there are three 1,10-phen chelators in **4** compared to two 1,10-phen ligands in **5**, and d) as a result, there is one bound nitrato ligand in **4** as opposed to two nitrato groups in **5**. Even though the two tetranuclear clusters bear the same total number of ligands (8), the individual composition of each assembly differs in the relative number of ligands employed in each case. Inevitably, therefore, the number of counter acting nitrate ions in **4** and **5** differ significantly, thus reflecting potential differences owing to the variable oxidation state of the cobalt ions present in each corresponding assembly. Another major difference between **4** and **5** is the significant number of lattice molecules present, with methanol (**4**) and water (**5**) being pronouncedly evident. Undoubtedly, the two different employed molecular stoichiometries present an idiotypic yet distinct behavior of the ternary system, thereby reflecting a clear prevalence of that factor over temperature in the isolation of compounds **4** and **5**. Here, too, the structural speciation linked to molecular stoichiometry reflects the wealth of species present and potentially amenable to isolation under the employed experimental conditions (Table 5).

Evaluation of the two stoichiometries, under variable temperature conditions, reveals that a) the nuclearity of the clusters (4) is retained regardless of the temperature employed in the isolation of the compounds, b) the hydroxide and iminodipropanol ligand number is retained in both clusters, with the 1,10-phen and nitrate number being varied, and c) the oxidation state of the cobalt centers is different (2Co(II) and 2Co(III)) within both **4** and **5** (vide infra), thus projecting the influence of the deprotonation state of the ligand in dictating the charge of the overall assembly, with the same number of counteracting nitrate ions in **4** and **5**.

Phenanthroline appears to have a discrete impact on the structural speciation of the ternary system investigated despite the salient features common with 2,2′-bipy.

The case of 4,4′-bipy entering the investigated ternary system is totally different from that in the case of 2,2′-bipy. Employment of a 2:1:1 stoichiometry at 4°C led to the isolation of compound **6**. In contrast to what had been observed with 2,2′-bipy, the isolated compound was a coordination polymer not containing iminodipropanol, but instead involving 4,4′-bipy, two nitrates and two water molecules, overall formulating an octahedral environment around Co(II). No changes in the oxid-

ation state of Co(II) were observed in **6** as in the previous cases of clusters **1–5**. In all cases of compounds studied, structural attributes of the variably configured mononuclear, trinuclear and tetranuclear assemblies reflected upon the inherent properties of the metal-organic assemblies through elaboration of the Hirshfeld surfaces in the corresponding species **1–6**. Careful examination of the arising d_{norm}, shape index and curvedness supplemented by 2D-fingerprint plots provided significant insight into modes of interactions, involving Van der Waals, H-bond and C-H···π and π···π profiles of adjacently located moieties (i.e. structural components inside the surfaces, counterions, lattice solvent molecules, etc.) in the studied clusters. As a consequence of the sensitivity linked to studying Hirshfeld surfaces, the accrued individual and collective information emphasized the contributions of the involved interactions to the architecture and lattice attributes of **1–6**, thus complementing the structural speciation study of the investigated systems.

Parameterization of Factors Contributing to Lattice Differentiation and Dimensionality

The structural parameters emerging as factors in the architecture of the arising mononuclear and oligonuclear assembles in **1–6**, involve the nuclearity, dimensionality of the arising lattice, oxidation state of the Co centers within each assembly, and nature of the bridging ligands in each assembly (OH^- vs. H_2O or CH_3O^-). Taking into consideration the potential contributors in the architecture of **1–6**, thus shaping the arising lattices, the following observations can be made: a) there is one mononuclear compound of polymeric nature (**6**), two trinuclear compounds (**2** and **3**), and three tetranuclear compounds (**1**, **4**, and **5**); b) the oxidation states of the cobalt centers comprising the arising assemblies are: two Co(III) and two Co(II) centers for **1**, **4**, and **5**, two Co(III) and one Co(II) centers in **2** and **3**, and one Co(II) center in **6**. It appears therefore, that the trend is uniform in the entire series (i.e. two Co(III) and two Co(II) centers) of tetranuclear assemblies, with one Co(II) center abstaining from the assembly when nuclearity is reduced by 1. Thus, the presence of two Co(III) centers appears to be the basis pair of centers in each arising assembly. To that end, it'd be worth looking into the possibility of finding the synthetic reaction conditions and thus the reasons for such a need of a Co(II) center, when the nuclearity of the assembly increases to four; c) there appears to be no obvious correlation between the presence of distinct nature bridging ligands in the tetranuclear assemblies **1**, **4**, and **5,** and the dimensionality of the arising lattice architecture. Specifically, the constantly observed bridging ligand present in all species is the OH^- group. When the second bridge becomes an OH^- or CH_3O^- group, dimensionality goes from 1D (**1**) to 3D (**4**) and zero (**5**); d) in the case of compounds **2** and **3**, it appears that when the second bridge is a water molecule, the dimensionality of the emerging lattice rises from 1D (**2**) to 2D (**3**) upon deprotonation of the water molecule; e) in the case of compounds **4** and **5**, where all of the basic features mentioned above are retained, dimensionality is reduced on going from **4** to **5** (from 3D to zero) dramatically, thereby reflecting the potential contributions of the absence of a 1,10-phen, presence of an additional nitrato ligand and (de)protonation state of the second iminodipropanol ligand to the erection of the cluster assembly, along the interplay of hydrophobic, bulk and hydrogen-bonding interactions, collectively configuring lattice architecture. The reduction of the number of 1,10-phen ligands, increase of the nitrato ligands, and decrease of the deprotonation state of the iminodipropanol ligand seem to favor reduction of lattice dimensionality from 3D (**4**) to zero (**5**). The mononuclear assembly in **6** bears distinct features allowing development of a 2D lattice in the emerging polymeric coordination environment, an ostensible disentanglement from obvious structural features present in all other assemblies **1–5**. Evidently, the three dimensional lattice in **4** appears to be the highest achieved among all tetranuclear assemblies bearing the aforementioned characteristics, thus projecting the interwoven contributions of the above factors in the formulation of the lattice architecture, more so than in the other tetranuclear and/or trinuclear assemblies.

Magneto-Structural Correlations

The majority of the compounds emerging from the studied ternary systems were trinuclear and tetranuclear. The magnetic susceptibility studies on **1**, **4** and **5** showed that the specific tetranuclear assemblies exhibit, in the temperature range investigated (1.8–320 K), behavior consistent with weak ferromagnetic interactions (1–2 cm^{-1}) between Co(II) ions. The structural arrangement of the cobalt centers in **1**, **4** and **5** stands different from that observed in tetranuclear complexes of the type $\{[Co^{II}_2Co^{III}_2(HL)_2(OCH_3)_2(N_3)_3]ClO_4{\cdot}5H_2O{\cdot}CH_3OH\}_n$ (**7**), $\{[Co^{II}_2Co^{III}_2(HL)_2(OCH_3)_2(N_3)_3]Cl{\cdot}H_2O\}_n$ (**8**) (H_3L=2,6-bis[(2-hydroxy-ethylimino)-methyl]-4-methylphenol),[37] also projecting cationic assemblies and containing mixed oxidation state cobalt ions in an overall similar cluster structure. The Co(III) centers (low spin) in these clusters stand at a distance of 3.004 (**7**) and 2.971 Å (**8**), with the Co(II) centers (high spin) spanning distances of around 5.480 Å, and both metric arrangements being diametrically opposed to the ones observed in our case (Co(III)···Co(III): 5.290 Å (**1**), 5.287 Å (**4**), 5.244–5.297 Å (**5**); Co(II)···Co(II): 3.068 Å (**1**), 3.090 Å (**4**), 3.062–3.076 Å (**5**)). In this regard, the magnetic profile of **1**, **4** and **5** is quite distinct from that seen in **7**, where the observed χ_m vs. T behavior reflects two non-interacting Co(II) centers in the cluster assembly. A similar structural arrangement of mixed oxidation state cobalt ions in a $[(Co^{II}_2Co^{III}_2L_4(H_2O)_2(CH_3COO)_2]^0$ (**9**) cluster, containing a doubly deprotonated form of the ligand H_2L [1-(3-hydroxypropyliminomethyl)naphthalene-2-ol] and alkoxido bridges, led to the observation of a different χ_m vs. T behavior reflecting antiferromagnetically coupled Co(II) ions (high spin) (Co(II)···Co(II) 3.206 Å) mediated by alkoxido bridges, with the Co(III) centers being low spin (Co(III)···Co(III) 5.231 Å).[38] Undoubtedly, the presence of distinctly differentiated ligands (H_3L and azide in **7** and **8**, H_2L and alkoxido moieties in **9**, and iminodipropanol and 2,2′-bipy and 1,10-phen in **1**, **4** and **5**), entering the assembly of similar type of cationic clusters, stands as a crucial factor in ultimately dictating a structurally linked and uniquely defined magnetic behavior. A more in-depth look at this family of spe-

Full Paper
doi.org/10.1002/ejic.202000435

cies is warranted to unravel new information on magnetically distinct cluster assemblies of the type described in this work.

The so derived interactions were supported by EPR measurements in the 2–20 K range. Given that all of the above species were tetranuclear, changes observed in the ferromagnetic profile may be related to the composition of their structure. In that sense, one observes that the highest and lowest $\chi_M T$ values appear in the profile of compound **4**. In view of the fact that a) the bridging ligands ((OH^-) and (CH_3O^-)), b) the change from 2,2′-bipy to 1,10-phen, and c) the deprotonation state of the iminodipropanol ligands bound to the cobalt ions, are major contributors to the structural identity of **1**, **4**, and **5**, it appears that the specific factors were also linked to the magnetic susceptibility behavior of the species examined. Given, also, that the exchange interactions were of the magnitude of 2 cm^{-1} for **1** and **4**, with **4** displaying the highest lattice dimensionality (3D), ultimately being lowered to zero in **5** (exhibiting exchange interactions close to 1 cm^{-1}), it appears that **4** contains a better formulated rendition of a tetranuclear Co_4 structure with iminodipropanol and 1,10-phen than **5**. It should be pointed out that these observations are correlation trends in need of further perusal. In the case of polymeric **6**, a simple magnetic susceptibility behavior, for the same temperature range studied, was observed, consistent with a high spin Co(II) center. Interestingly enough, the frozen solution behavior of the tetranuclear complexes suggests, through EPR spectroscopy, that the solid state species do not retain their original structure in solution, thereby providing a deeper look into their solid state solution state correlation. The collective behavior sets the basis for further examination of the solution speciation of the investigated systems (vide supra) in this work, further facilitating the design and synthesis of new materials with improved magnetic profiles (vide infra).

Luminescence Properties

The presence of aromatic ligands, N,N′-chelators 2,2′-bipy and 1,10-phen, in the assembly of tetranuclear Co(II,III) clusters, suggested that the electronic luminescent properties be investigated. To that end, clusters **1**, **4** and **5** exhibited well-resolved features a) discretely differentiating the presence of the aromatic ligands bound to the cobalt centers, thus projecting the contribution of those ligands to the electronic properties of the individual clusters, and b) displaying quenched luminescence with respect to the free aromatic ligand binders, thus pointing out the importance of ligand binding to the formulation of the electronic profile of the cluster-specific assembly. On the basis of the structural characteristics of clusters **1**, **4** and **5**, the common feature is the distinct luminescence signature arising in connection with the identity of species. Albeit, starkly differentiated from **1–5**, polymeric compound **6** also exhibited quenched luminescence behavior, consistent with the presence of the aromatic 4,4′-bipy ligand binder, despite the fact that there is no chelating potential as in 2,2′-bipy and 1,10-phen counterparts encountered in the **1–5**.

Conclusions

The temperature-sensitive investigation of ternary systems of Co(II):iminodipropanol containing aromatic chelators 2,2′-bipy and 1,10-phen in alcoholic media (methanol) led to a surprising family of tetranuclear and trinuclear species, all of which were isolated in crystalline form. Analytical, spectroscopic and structural characterization of compounds **1–6** revealed a distinct influence of a) the molecular stoichiometry (1:1:1 and 2:1:1) of the investigated system, and b) temperature (4 and 25°C), over the nature of the compounds isolated from the reaction mixtures studied. The discrete identity of the species isolated in the course of the interplay of tested experimental conditions, testifies to the variable yet plethoric complex nature of structural speciation emerging as a result of the investigated chemical reactivity in the title ternary systems. In-depth elaboration of the structural speciation, established chemically in the investigated systems, was greatly enhanced by bond valence sum calculations and Hirshfeld surface analysis, providing credence to the crystallographic details of cluster interactions at the atomic and molecular level in the arisen architecture and lattice formation. The discrete identity of species in 2,2′-bipy vs. 1,10-phen ternary systems suggests that established physicochemical factors dictate the isolation of thermodynamically stable compounds **1–6**, thus contributing to the wealth of spectroscopic, structural, electrochemical, and magnetic properties of the well-defined materials of variable yet discrete nuclearity and oxidation state of the cobalt centers emerging in the clusters isolated. The observed collective data on the investigated systems formulate structure-lattice, structure-electronic and magnetic behavioral profiles, setting the parameterization for the design and synthesis of new materials with specified optical and magnetostructural properties.

Experimental Section

Materials and Methods: All manipulations were carried out under aerobic conditions. The following starting materials were used without further purification. Cobalt(II) nitrate hexahydrate $Co(NO_3)_2 \cdot 6H_2O$ was purchased from BDH Chemicals Ltd, 1,1′-iminodi-2-propanol (H_3L; Imino) from Merck-Schuchardt and 4,4′-bipyridine (4,4′-bipy) from Fluka AG. 2,2′-Bipyridine (2,2′-bipy), 1,10-phenanthroline (1,10-phen) as well as methanol were supplied by Sigma-Aldrich.

Physical Measurements: FT-IR spectra were recorded on a Thermo-Finnigan FT-Infra Red IR-200 spectrometer, using KBr pellets. UV/Visible measurements were carried out on a Hitachi U2001 spectrophotometer in the range from 190 to 900 nm. A Thermo Finnigan Flash EA 1112 CHNS elemental analyser was used for the simultaneous determination of carbon, hydrogen, and nitrogen (%). The analyser operation is based on the dynamic flash combustion of the sample (at 1800 °C) followed by reduction, trapping, complete GC separation and detection of the products. The instrument is a) fully automated and controlled by PC via the Eager 300 dedicated software, and b) capable of handling solid, liquid or gaseous substances.

Electron Paramagnetic Resonance: Electron paramagnetic resonance (EPR) measurements were performed on an upgraded X-band Bruker ER-200D spectrometer interfaced to a personal com-

puter and equipped with an Oxford ESR 900 cryostat, an Anritsu MF76A frequency counter and a Bruker 035M NMR gaussmeter. The Signal-Channel unit was replaced by an SR830 digital lock-in amplifier by Stanford Research. The EPR spectra of complexes **1–5** in the solid-state and in frozen aqueous solutions were typically recorded at microwave frequency of ca. 9.42 GHz and modulation amplitude of 5 to 25 Gpp at 100 kHz, with a microwave power of 20 mW and in the temperature range from 4.2 to 70 K.

Magnetic Susceptibility: Magnetic susceptibility measurements were performed on powdered polycrystalline materials, with an MPMS 7XL SQUID magnetometer (Quantum Design), working in the temperature range from 1.8 to 320 K, under external magnetic fields of 0.1 and 1.0 Tesla. Magnetization measurements were carried out in the field range 0–7 T and at T 2 K. The observed susceptibility data were corrected for the underlying diamagnetism.

Cyclic Voltammetry: Electrochemical measurements on all compounds (**1**,**4–6**) were carried out at room temperature in methanol, with an Autolab model PGSTAT302 potensiostat-galvanostat. The entire system was under computer control and supported by the appropriate computer Autolab software GPES, running on Windows. The electrochemical cell used had platinum (disk) working and auxiliary (wire) electrodes. As a reference electrode, a saturated Ag/$AgNO_3$ electrode was used. The solvent methanol used in the electrochemical measurements was of HPLC quality. Tetrabutylammonium perchlorate $(Bu_4N)ClO_4$ was used as a supporting electrolyte. The operation of the electrochemical cell was checked through the use of the $Fe(C_5H_5)_2/[Fe(C_5H_5)_2]^+$ reference system in the same solvent. Normal concentrations used were 1–2 mM in electroanalyte and 0.1 M in supporting electrolyte. Purified argon was used to purge the solutions prior to the electrochemical measurements.

Photoluminescence: Emission and excitation spectra were recorded on a Hitachi F-7000 fluorescence spectrophotometer from Hitachi High-Technologies Corporation. The employed split widths (em, ex) were 5.0 nm and the scan speed was 1200 nm min^{-1}. All measurements were carried out at room temperature. The entire system was supported by the appropriate computer software, FL Solutions 2.1, running on Windows XP.

Theoretical Calculations: Bond Valence Sum (BVS) calculations were carried out using the Visualization for Electronic and Structural Analysis (VESTA) program (Version 3.4.8).[61] Bond valence values (S) were obtained using the empirical expression $S = \exp[(R_o - r)/b]$, where b = 0.37 Å, r is the observed bond length and R_o (Å) is a tabulated constant. In our case, literature[62,63] R_o values are as follows: Co(II)–O 1.685, Co(III)–O 1.637, Co(II)-N 1.72 and Co(III)-N 1.69.

Hirshfeld Surface Analysis: Hirshfeld surface analysis,[64–66] depicting electron density boundary surfaces between molecules in a crystal, was carried out to interpret the presence of various intermolecular interactions present in all compounds studied. Hirshfeld surfaces and associated two-dimensional (2D) fingerprint[67,68] plots were calculated using Crystal Explorer,[69] with bond lengths to hydrogen atoms set to standard values.[70] During mapping, the derived surfaces were kept transparent for the visualization of various intermolecular interactions associated with self-assembly.

In the course of the analysis on a complex molecular assembly, an emerging isosurface is obtained. Each point of the isosurface can be defined by two distances: a) d_e, the distance from the point to the nearest atom outside the surface, and b) d_i, the distance to the nearest atom inside to the surface. Regions of particular importance to intermolecular interactions can be identified by mapping the normalized contact distance (d_{norm})

$$d_{norm} = \frac{(d_i - r_i^{vdw})}{r_i^{vdw}} + \frac{(d_e - r_e^{vdw})}{r_e^{vdw}}$$

Where r_i^{vdw} and r_e^{vdw} are the van der Waals radii of the atoms. The value of d_{norm} can be either negative or positive, when intermolecular contacts are shorter or longer than r^{vdw}, respectively. Hirshfeld surface plots, mapped with d_{norm}, display blue-red-white color graphics. Red color indicates shorter intermolecular contacts, white color reflects contacts around the r^{vdw} separation, and blue color indicates longer contact distances. Due to symmetry between d_e and d_i in the mathematical expression for d_{norm}, where two Hirshfeld surfaces come in contact, they both exhibit a red spot identical in color intensity, size and shape.[71] Furthermore, close contacts between specific atom types can be highlighted in resolved fingerprint plots,[43,67,68] thereby allowing facile assignment of an intermolecular contact to a specific type of interaction. Two additional colored attributes (shape index and curvedness), based on the local curvature of the generated surface, can also be specified.[72] Two dimensional fingerprint plots of each Hirshfeld surface were derived so as to project d_{norm}, shape-index, curvedness and 2D fingerprint plots (full and resolved), with plots of d_i vs. d_e contributing to understanding of the different intermolecular interactions emerging in each case of crystal structure investigated.

Synthesis

Ternary system: Co(II)-Imino-2,2′-bipy

Solvent: Methanol

Molecular stoichiometry:1:1:1

Reaction temperature:25°C

Synthesis of $[Co^{II}_2Co^{III}_2(OH)(CH_3O)(C_6H_{12.5}NO_2)_2(C_{10}H_8N_2)_2(NO_3)_2](NO_3)\cdot 3CH_3OH\cdot H_2O$ (1): $Co(NO_3)_2\cdot 6H_2O$ (0.30 g, 1.0 mmol) was dissolved in 5 mL of methanol in a 25 mL round-bottomed flask. To that, a solution of 1,1′-iminodi-2-propanol (Imino) (0.14 g, 1.0 mmol) in 2 mL of methanol was added. The resulting dark red reaction mixture was stirred at room temperature for 10 min. Subsequently, 2,2′-bipy (0.16 g, 1.0 mmol) was added slowly to the reaction mixture under continuous stirring. The emerging reaction solution was filtered and allowed to stand at 25°C. After a couple of days, dark red crystals grew out of solution. The crystalline material was collected by filtration and dried in vacuo. Yield: 0.080g (ca. 26 %). Anal. Calc. for **1**, ($C_{36}H_{59}Co_4N_9O_{19}$ MW=1157.65): C, 37.36; H, 5.14; N, 10.89; found C, 37.41; H, 5.14; N, 10.80 %.

Reaction temperature:4°C

Synthesis of $[Co^{II}Co^{III}_2(H_2O)(OH)(C_6H_{13}NO_2)_2(C_{10}H_8N_2)_3](NO_3)_3\cdot 2CH_3OH$ (2) and $[Co^{II}Co^{III}_2(OH)_2(C_6H_{14}NO_2)_2(C_{10}H_8N_2)_3](NO_3)_4\cdot CH_3OH$ (3): The reaction was run as in the aforementioned preparation. The final reaction solution was filtered and allowed to stand at 4°C. After a short period of time, dark red crystals grew out of the solution by slow evaporation. The product was isolated by filtration and dried in vacuo. Yield: 0.090 g. Repeated synthetic efforts led to the identity of the product being a mixture of compounds **2** and **3**, as confirmed by X-ray crystallography. Anal. Calc. for **2**, ($C_{44}H_{53}Co_3N_{11}O_{17}$ MW=1184.77) and **3**, ($C_{43}H_{58}Co_3N_{12}O_{19}$ MW=1223.80).

Molecular stoichiometry:2:1:1

Reaction temperature:25°C

Synthesis of $[Co^{II}_2Co^{III}_2(OH)(CH_3O)(C_6H_{12.5}NO_2)_2(C_{10}H_8N_2)_2(NO_3)_2](NO_3)\cdot 3CH_3OH\cdot H_2O$ (1): $Co(NO_3)_2\cdot 6H_2O$ (0.60 g, 2.0 mmol) was dissolved in 5 mL of methanol and a solution of 1,1′-iminodi-

2-propanol (Imino) (0.14 g, 1.0 mmol) in 2 mL of methanol was added to that in a 25 mL round-bottomed flask. The dark red reaction mixture was then stirred at room temperature for 10 min. Next, 2,2′-bipy (0.16 g, 1.0 mmol) was added slowly to the reaction mixture under continuous stirring. Subsequently, the reaction solution was filtered and allowed to stand at 25°C. After a day or so, dark red crystals grew out of the solution. The product was isolated by filtration and dried in vacuo. Yield: 0.070 g (ca. 12 %). Anal. Calc. for **1**, ($C_{36}H_{59}Co_4N_9O_{19}$ MW=1157.65): C, 37.36; H, 5.14; N, 10.89; found C, 37.31; H, 5.16; N, 10.87 %.

Reaction temperature:4°C

Synthesis of $[Co^{II}_2Co^{III}_2(OH)(CH_3O)(C_6H_{12.5}NO_2)_2(C_{10}H_8N_2)_2(NO_3)_2](NO_3)\cdot 3CH_3OH\cdot H_2O$ (1): The reaction was run with the same reagent molecular stoichiometry as in the aforementioned preparation at 25°C. The final reaction solution was filtered and allowed to stand at 4°C. After a day or so, dark red crystals grew out of the solution. The product was isolated by filtration and dried in vacuo. Yield: 0.030 g (5 %). Anal. Calc. for **1**, ($C_{36}H_{59}Co_4N_9O_{19}$ MW= 1157.65): C, 37.36; H, 5.14; N, 10.89; found C, 37.26; H, 5.12; N, 10.82 %.

Ternary system:Co(II)-Imino-(1,10-phen)

Solvent:Methanol

Molecular stoichiometry:1:1:1

Reaction temperature:25°C

Synthesis of $[Co^{II}_2Co^{III}_2(OH)_2(C_6H_{12.5}NO_2)_2(C_{12}H_8N_2)_3(NO_3)](NO_3)_2\cdot 3CH_3OH$ (4): $Co(NO_3)_2\cdot 6H_2O$ (0.60 g, 2.0 mmol) was dissolved in 5 mL of methanol and 1,1′-iminodi-2-propanol (Imino) (0.28 g, 2.0 mmol) in 2 mL of methanol. Then, the two reagents were mixed in a 25 mL round-bottomed flask and the arising reaction mixture was stirred at room temperature for 10 min. Next, 1,10-phenanthroline (0.36 g, 2.0 mmol) was added very slowly under continuous stirring. Subsequently, the emerging reaction solution was filtered and allowed to stand at 25°C. After a short period of time, dark brown crystals grew out of the solution. The product was isolated by filtration and dried in vacuo. Yield: 0.17g (ca. 25 %). Anal. Calc. for **4**, ($C_{51}H_{56}Co_4N_{11}O_{18}$ MW=1346.80): C, 45.48; H, 4.19; N, 11.44; found C, 45.40; H, 4.14; N, 11.39 %.

Reaction temperature:4°C

Synthesis of $[Co^{II}_2Co^{III}_2(OH)_2(C_6H_{12.5}NO_2)_2(C_{12}H_8N_2)_3(NO_3)](NO_3)_2\cdot 3CH_3OH$ (4): The reaction was run with the same reagent molecular stoichiometry as in the aforementioned preparation at 25°C. The final reaction solution was filtered and allowed to stand at 4°C. After a day or so, dark brown crystals grew out of the solution. The product was isolated by filtration and dried in vacuo. Yield: 0.14 g (ca. 20 %). Anal. Calc. for **4**, ($C_{51}H_{56}Co_4N_{11}O_{18}$ MW=1346.80): C, 45.48; H, 4.19; N, 11.44; found C, 45.44; H, 4.17; N, 11.47 %.

Molecular stoichiometry: 2:1:1

Reaction temperature:25°C

Synthesis of $[Co^{II}_2Co^{III}_2(OH)_2(C_6H_{13}NO_2)_2(C_{12}H_8N_2)_2(NO_3)_2](NO_3)_2\cdot 2.5H_2O$ (5): $Co(NO_3)_2\cdot 6H_2O$ (0.60 g, 2.0 mmol) and 1,1′-iminodi-2-propanol (0.14 g, 1.0 mmol) were dissolved in 5 mL and 2 mL of methanol, respectively, in a 25 mL round-bottomed flask under continuous stirring. The resulting reaction mixture was then stirred at room temperature for 10 min. Next, 1,10-phenanthroline (0.18 g, 1.0 mmol) was added very slowly to the reaction mixture under continuous stirring. Subsequently, the emerging reaction solution was filtered and allowed to stand at 25°C. After a couple of days, dark brown crystals grew out of the solution by slow evaporation. The product was isolated by filtration and dried in vacuo. Yield: 0.10 g (ca. 16 %). Anal. Calc. for **5**, ($C_{36}H_{49}Co_4N_{10}O_{20.50}$ MW=1185.57): C, 36.44; H, 4.13; N, 11.81; found C, 36.40; H, 4.17; N, 11.78 %.

Reaction temperature:4°C

Synthesis of $[Co^{II}_2Co^{III}_2(OH)_2(C_6H_{13}NO_2)_2(C_{12}H_8N_2)_2(NO_3)_2](NO_3)_2\cdot 2.5H_2O$ (5): The reaction was run with the same reagent molecular stoichiometry as in the aforementioned preparation at 25°C. The final reaction solution was filtered and allowed to stand at 4°C. After a day or so, dark brown crystals grew out of the solution. The product was isolated by filtration and dried in vacuo. Yield: 0.05 g (ca. 8 %). Anal. Calc. for **5**, ($C_{36}H_{49}Co_4N_{10}O_{20.50}$ MW=1185.57): C, 36.44; H, 4.13; N, 11.81; found C, 36.42; H, 4.17; N, 11.83 %.

Ternary system:Co(II)-Imino-(4,4′-bipy)

Solvent:Methanol

Molecular stoichiometry:2:1:1

Reaction temperature:4°C

Synthesis of $[Co^{II}(C_{10}H_8N_2)(NO_3)_2(H_2O)_2]_n$ nH_2O (6): $Co(NO_3)_2\cdot 6H_2O$ (0.60 g, 2.0 mmol) and 1,1′-iminodi-2-propanol (Imino) (0.14 g, 1.0 mmol) were placed in a 25 mL round-bottomed flask and 5 mL of methanol was added under continuous stirring. The reaction mixture was then stirred at room temperature until both reactants were completely dissolved. Furthermore, 4,4′-bipy (0.16 g, 1.0 mmol) was placed in 2 mL of methanol and then was added drop by drop to the reaction mixture under continuous stirring. Subsequently, the emerging reaction solution was filtered and allowed to stand at 4°C. After six days, pink prismatic crystals grew out of the solution by slow evaporation. The crystalline material was collected by filtration and dried in vacuo. Yield: 0.19 g (ca. 23 %). Anal. Calcd for **6**, ($C_{10}H_{14}CoN_4O_9$ MW=393.18): C, 30.55; H, 3.59; N, 14.25; found C, 30.60; H, 3.60; N, 14.36 %.

Reaction temperature:25°C

Synthesis of $[Co^{II}(C_{10}H_8N_2)(NO_3)_2(H_2O)_2]_n\cdot nH_2O$ (6): The reaction was run with the same reagent molecular stoichiometry as in the aforementioned preparation at 25°C. The final reaction solution was filtered and allowed to stand at 25°C. After two to three days, microcrystalline material grew out of the solution by slow evaporation. The product was isolated by filtration and dried in vacuo. Yield: 0.19 g (ca. 23 %). Anal. Calcd for **6**, ($C_{10}H_{14}CoN_4O_9$ MW=393.18): C, 30.55; H, 3.59; N, 14.25; found C, 30.58; H, 3.54; N, 14.21 %. The material was further identified as **6** by FT-IR.

X-ray Crystal Structure Determination: Single crystals of compounds **1–6** were obtained from reaction mixtures according to the described synthetic procedures. For the structural determination of **1–6**, single crystals of the respective compounds were mounted on a Bruker Kappa APEX II diffractometer, equipped with a triumph monochromator at ambient temperature. Diffraction measurements were recorded using Mo K_α radiation. Unit cell dimensions were determined by using at least 100 reflections in the range $15 < \theta < 20°$. Intensity data were collected using φ and ω scan mode. The frames collected for each crystal were integrated with the Bruker SAINT software package[73] using a narrow-frame algorithm. Data were corrected for absorption using the numerical method (SADABS) based on crystal dimensions.[74]

All structures were solved using the SUPERFLIP[75] package and refined by full–matrix least-squares method on F^2 using the CRYSTALS package versions 14.43 and 14.61.[76] All non-disordered non-hydrogen atoms were refined anisotropically.

All hydrogen atoms, except for the ones being disordered, were found at their expected positions and refined using soft constraints. By the end of the refinement, they were positioned using riding

constraints. The crystal data, details of data collection and structure refinement for all compounds studied are given in Table 1. Illustrations were drawn by CAMERON[77] and Diamond.[78] Further details on the crystallographic studies as well as atomic displacement parameters are given as Supporting Information.

Deposition Numbers 1999633 (for **1**), 1999634 (for **2**), 1999635 (for **3**), 1999636 (for **4**), 1999637 (for **5**), and 1999638 (for **6**) contain the supplementary crystallographic data for this paper. These data are provided free of charge by the joint Cambridge Crystallographic Data Centre and Fachinformationszentrum Karlsruhe Access Structures service www.ccdc.cam.ac.uk/structures.

Conflicts of interest

The authors declare no conflict of interest.

Keywords: Cobalt · Cluster compounds · Metal-organic materials · Synthesis design · Magnetic properties · Structure-activity relationships

[1] T. Kuroda-Sowa, M. Lamm, A. L. Rheingold, C. Frommen, W. M. Reiff, M. Nakano, J. Yoo, A. L. Maniero, L. C. Brunel, G. Christou, D. N. Hendrickson, *Inorg. Chem.* **2001**, *40*, 6469–6480.
[2] L. Fu, L. Chen, H. Yuan, Y. Chen, B. Li, *Inorg. Chem. Commun.* **2019**, *106*, 180–184.
[3] L. Chun, C. R. Kagan, *J. Am. Chem. Soc.* **2003**, *125*, 336–337.
[4] L. Bogani, W. Wernsdorfer, *Nat. Mater.* **2008**, *7*, 179–186.
[5] E. Coronado, J. R. Galán-Mascarós, C. J. Gómez-García, V. Laukhin, *Nature* **2000**, *408*, 447–449.
[6] X. Yang, S. Wang, L. Zhang, C. Wang, T. Zhu, L. Bo, S. Huang, *Nanoscale* **2017**, *9*, 517–521.
[7] A. Donmez, G. Oylumluoglu, M. B. Coban, C. Kocak, M. Aygun, H. Kara, *J. Mol. Struct.* **2017**, *1149*, 569–575.
[8] M. Kurmoo, *Chem. Soc. Rev.* **2009**, *38*, 1353–1379.
[9] G. A. Craig, M. Murrie, *Chem. Soc. Rev.* **2015**, *44*, 2135–2147.
[10] Y. Z. Zheng, G. J. Zhou, Z. Zheng, R. E. P. Winpenny, *Chem. Soc. Rev.* **2014**, *43*, 1462–1475.
[11] M. J. Byrnes, M. H. Chisholm, N. J. Patmore, *Inorg. Chem.* **2005**, *44*, 9347–9352.
[12] P. F. Yao, Y. K. Chen, C. F. Lai, H. Y. Li, H. D. Bian, H. F. Liu, D. Yao, F. P. Huang, *Inorg. Chem.* **2018**, *57*, 9182–9189.
[13] M. Schweiger, S. R. Seidel, M. Schmitz, P. J. Stang, *Org. Lett.* **2000**, *2*, 1255–1257.
[14] Z. L. You, H. L. Zhu, *Z. Anorg. Allg. Chem.* **2004**, *630*, 2754–2760.
[15] N. Raman, C. Thangaraja, S. Johnsonraja, *Cent. Eur. J. Chem.* **2005**, *3*, 537–555.
[16] S. Shaygan, H. Pasdar, N. Foroughifar, M. Davallo, F. Motiee, *Appl. Sci.* **2018**, *8*, 385.
[17] A. K. Singh, S. Kumari, T. N. Guru Row, J. Prakash, K. Ravi Kumar, B. Sridhar, T. R. Rao, *Polyhedron* **2008**, *27*, 3710–3716.
[18] M. Du, C. P. Li, C. S. Liu, S. M. Fang, *Coord. Chem. Rev.* **2013**, *257*, 1282–1305.
[19] R. Q. Zou, H. Sakurai, Q. Xu, *Angew. Chem. Int. Ed.* **2006**, *45*, 2542–2546; *Angew. Chem.* **2006**, *118*, 2604.
[20] T. Tao, Y. H. Lei, Y. X. Peng, Y. Wang, W. Huang, Z. X. Chen, X. Z. You, *Cryst. Growth Des.* **2012**, *12*, 4580–4587.
[21] M. Menelaou, M. Daskalakis, A. Mateescu, C. P. Raptopoulou, A. Terzis, C. Mateescu, V. Tangoulis, T. Jakusch, T. Kiss, A. Salifoglou, *Polyhedron* **2011**, *30*, 427–437.
[22] S. Karasawa, K. Nakano, D. Yoshihara, N. Yamamoto, J. I. Tanokashira, T. Yoshizaki, Y. Inagaki, N. Koga, *Inorg. Chem.* **2014**, *53*, 5447–5457.
[23] S. Chattopadhyay, G. Bocelli, A. Musatti, A. Ghosh, *Inorg. Chem. Commun.* **2006**, *9*, 1053–1057.
[24] C. Tian, Z. Lin, S. Du, *Cryst. Growth Des.* **2013**, *13*, 3746–3753.
[25] T. Shiga, H. Oshio, *Polyhedron* **2007**, *26*, 1881–1884.
[26] M. Dincă, T. D. Harris, A. T. Iavarone, J. R. Long, *J. Mol. Struct.* **2008**, *890*, 139–143.
[27] J. P. Zhao, W. C. Song, R. Zhao, Q. Yang, B. W. Hu, X. H. Bu, *Cryst. Growth Des.* **2013**, *13*, 2858–2865.
[28] K. W. Galloway, A. M. Whyte, W. Wernsdorfer, J. Sanchez-Benitez, K. V. Kamenev, A. Parkin, R. D. Peacock, M. Murrie, *Inorg. Chem.* **2008**, *47*, 7438–7442.
[29] K. Chakarawet, P. C. Bunting, J. R. Long, *J. Am. Chem. Soc.* **2018**, *140*, 2058–2061.
[30] V. Chandrasekhar, A. Dey, A. J. Mota, E. Colacio, *Inorg. Chem.* **2013**, *52*, 4554–4561.
[31] V. Tudor, A. Madalan, V. Lupu, F. Lloret, M. Julve, M. Andruh, *Inorg. Chim. Acta* **2010**, *363*, 823–826.
[32] R. Gheorghe, G. A. Ionita, C. Maxim, A. Caneschi, L. Sorace, M. Andruh, *Polyhedron* **2019**, *171*, 269–278.
[33] T. S. Mahapatra, D. Basak, S. Chand, J. Lengyel, M. Shatruk, V. Bertolasi, D. Ray, *Dalton Trans.* **2016**, *45*, 13576–13589.
[34] A. Ghisolfi, K. Y. Monakhov, R. Pattacini, P. Braunstein, X. López, C. De Graaf, M. Speldrich, J. van Leusen, H. Schilderb, P. Kögerler, *Dalton Trans.* **2014**, *43*, 7847–7859.
[35] E. Martin, V. Tudor, A. M. Madalan, C. Maxim, F. Tuna, F. Lloret, M. Julve, M. Andruh, *Inorg. Chim. Acta* **2018**, *475*, 98–104.
[36] X. Y. Wang, S. C. Sevov, *Inorg. Chem.* **2008**, *47*, 1037–1043.
[37] S. S. Tandon, S. D. Bunge, R. Rakosi, Z. Xu, *Dalton Trans.* **2009**, 6536–6551.
[38] M. B. Coban, E. Gungor, H. Kara, U. Baisch, Y. Acar, *J. Mol. Struct.* **2018**, *1154*, 579–586.
[39] P. King, R. Clérac, W. Wernsdorfer, E. Anson, A. K. Powell, *Dalton Trans.* **2004**, 2670–2676.
[40] K. Ghosh, K. Harms, A. Bauzá, A. Frontera, S. Chattopadhyay, *CrystEngComm* **2018**, *20*, 7281–7292.
[41] S. Luachan, C. Pakawatchai, A. Rujiwatra, *J. Inorg. Organomet. Polym. Mater.* **2007**, *17*, 561–568.
[42] M. Felloni, A. J. Blake, N. R. Champness, P. Hubberstey, C. Wilson, M. Schröder, *J. Supramol. Chem.* **2002**, *2*, 163–174.
[43] A. L. Rohl, M. Moret, W. Kaminsky, K. Claborn, J. J. McKinnon, B. Kahr, *Cryst. Growth Des.* **2008**, *8*, 4517–4525.
[44] W. M. I. Hassan, M. A. Badawy, G. G. Mohamed, H. Moustafa, S. Elramly, *Spectrochim. Acta* **2013**, *111*, 169–177.
[45] M. M. Campos-Vallette, R. E. Clavijo, F. Mendizabal, W. Zmudio, R. Baraona, G. Diaz, *Vib. Spectrosc.* **1996**, *12*, 37–44.
[46] X.-M. Shi, H.-Y. Wang, Y.-B. Li, J.-X. Yang, L. Chen, G. Hui, W.-Q. Xu, B. Zhao, *Chem. Res. Chin. U.* **2010**, *26 (6)*, 1011-1015..
[47] K. Das, A. Datta, P. H. Liu, J. H. Huang, C. L. Hsu, W. T. Chang, C. Sina, *Polyhedron* **2014**, *71*, 85–90.
[48] S. Parveen, G. Velmurugan, E. Sinn, P. Venuvanalingam, S. Govindarajan, *J. Photochem. Photobiol. B* **2018**, *189*, 152–164.
[49] K. Nakamoto, *Infrared spectra of inorganic and coordination compounds*; John Wiley & Sons: New York, **1970**.
[50] R. A. Ahmadi, F. Hasanvand, G. Bruno, H. A. Rudbari, S. Amani, *ISRN Inorg. Chem.* **2013**, 1–7.
[51] N. Yaghoobi Nia, P. Farahani, H. Sabzyan, M. Zendehdel, M. Oftadeh, *Phys. Chem. Chem. Phys.* **2014**, *16*, 11481–11491.
[52] A. K. Pal, C. Li, G. S. Hanan, E. Zysman-Colman, *Angew. Chem. Int. Ed.* **2018**, *57*, 8027; *Angew. Chem.* **2018**, *130*, 8159–8163.
[53] W. H. Zhang, Z. Dong, Y. Y. Wang, L. Hou, J. C. Jin, W. H. Huang, Q. Z. Shi, *Dalton Trans.* **2011**, *40*, 2509–2521.
[54] L. Wang, J. Hao, L. X. Zhai, Y. Zhang, W. K. Dong, *Crystals* **2017**, *7*, 277.
[55] B. R. Fu, S. C. Xiang, S. M. Hu, L. S. Wang, Y. M. Li, X. H. Huang, X. T. Wu, *Chem. Commun.* **2005**, 5292–5294.
[56] R. Boca, *Coord. Chem. Rev.* **2004**, *248*, 757–815.
[57] R. L. Carlin, *Magnetochemistry*; Springer: Heidelberg, **1986**.
[58] A. Abragam, B. Bleaney, *In Electron Paramagnetic Resonance of Transition Ions*; Clarendon Press: Oxford, U. K. **1970**.
[59] N. F. Chilton, R. P. Anderson, L. D. Turner, A. Soncini, K. S. Murray, *J. Comput. Chem.* **2013**, *34*, 1164–1175.
[60] S. R. Hosseinian, V. Tangoulis, M. Menelaou, C. P. Raptopoulou, V. Psycharis, C. Dendrinou-Samara, *Dalton Trans.* **2013**, *42*, 5355–5366.
[61] K. Momma, F. Izumi, *J. Appl. Crystallogr.* **2011**, *44*, 1272–1276.
[62] R. M. Wood, G. J. Palenik, *Inorg. Chem.* **1998**, *37*, 4149–4151.
[63] I. D. Brown, *IUCrJ* **2017**, *4*, 514–515.
[64] M. A. Spackman, D. Jayatilaka, *CrystEngComm* **2009**, *11*, 19–32.

[65] S. L. Tan, M. M. Jotanib, E. R. T. Tiekink, *Acta Crystallogr., Sect. E:. Cryst. Commun.* **2019**, *75*, 308–318.
[66] H. F. Clausen, M. S. Chevallier, M. A. Spackman, B. B. Iversen, *New J. Chem.* **2010**, *34*, 193–199.
[67] M. A. Spackman, J. J. McKinnon, *CrystEngComm* **2002**, *4*, 378–392.
[68] A. Parkin, G. Barr, W. Dong, C. J. Gilmore, D. Jayatilaka, J. J. McKinnon, M. A. Spackman, C. C. Wilson, *CrystEngComm* **2007**, *9*, 648–652.
[69] M. J. Turner, J. J. McKinnon, S. K. Wolff, D. J. Grimwood, P. R. Spackman, D. Jayatilaka, M. A. Spackman, Crystal Explorer 17.5, The University of Western Australia, **2017**.
[70] F. H. Allen, O. Kennard, D. G. Watson, L. Brammer, A. Guy Orpen, R. Taylor, *J. Chem. Soc., Perkin Trans. 1* **1987**, *2*, S1–S19.
[71] I. D. Madura, J. Zachara, H. Hajmowicz, L. Synoradzki, *J. Mol. Struct.* **2012**, *1017*, 98–105.
[72] J. J. Koenderink, A. J. van Doorn, *Image Vision Comput.* **1992**, *10*, 557–564.
[73] Bruker Analytical X-ray Systems, *Inc. Apex2*, Version 2 User Manual, M86-E01078, Madison, WI, **2006**.
[74] Siemens Industrial Automation, Inc. *SADABS*: Area-Detector Absorption Correction; Madison, WI, **1996**.
[75] P. W. Betteridge, J. R. Carruthers, R. I. Cooper, K. Prout, D. J. Watkin, *J. Appl. Crystallogr.* **2003**, *36*, 1487.
[76] L. Palatinus, G. J. Chapuis, *J. Appl. Crystallogr.* **2007**, *40*, 786–790.
[77] D. J. Watkin, C. K. Prout, L. J. Pearce, *CAMERON*; Chemical Crystallography Laboratory: Oxford, U. K. **1996**.
[78] *DIAMOND – Crystal and Molecular Structure Visualization*, Ver. 3.1c, Crystal Impact, Bonn, Germany, **2006**.

Received: May 3, 2020

Full Paper
doi.org/10.1002/ejic.202000435

Chemistry Europe
European Chemical Societies Publishing

Cobalt Clusters

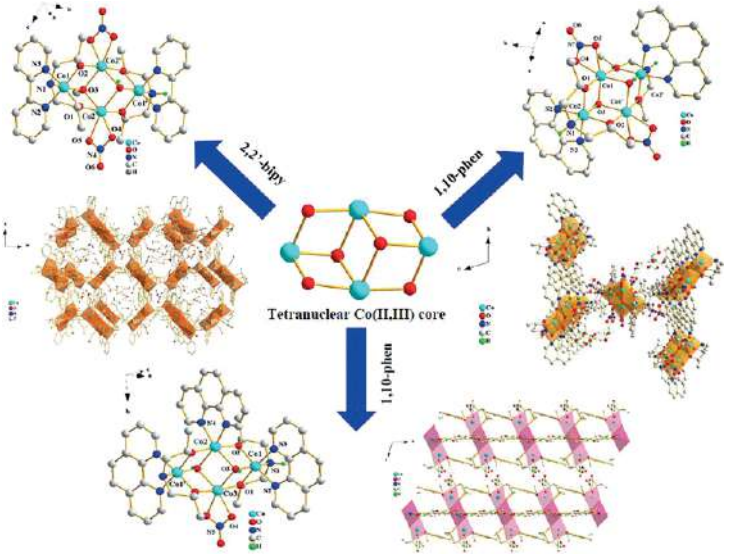

Structural speciation of Co(II):iminodipropanol:N,N′-aromatic chelator systems, under temperature-specific conditions, reveals binary-ternary hybrid metal-organic coordination compounds of mono-, tri-, and tetranuclear Co(II,III) centers. Octahedral Co(II,III) cluster arrangements project distinct optical and magnetic properties, thereby establishing lattice architecture-magneto-optical correlations useful in the development of advanced materials.

doi.org/10.1002/ejic.202000435